Dynamic regulation of gonadal transposon control across the lifespan of the naturally short-lived African turquoise killifish

Bryan B. Teefy[1], Ari Adler[1], Alan Xu[1,2], Katelyn Hsu[1,2], Param Priya Singh[3], Bérénice A. Benayoun[1,2,4,5,6,*]

[1] Leonard Davis School of Gerontology, University of Southern California, Los Angeles, CA 90089, USA.

[2] Molecular and Computational Biology Department, USC Dornsife College of Letters, Arts and Sciences, Los Angeles, CA 90089, USA.

[3] Department of Genetics, Stanford University, Stanford, CA, USA

[4] Biochemistry and Molecular Medicine Department, USC Keck School of Medicine, Los Angeles, CA 90089, USA.

[5] USC Norris Comprehensive Cancer Center, Epigenetics and Gene Regulation, Los Angeles, CA 90089, USA.

[6]USC Stem Cell Initiative, Los Angeles, CA 90089, USA.

[*] Corresponding author (berenice.benayoun@usc.edu).

Abstract

Although germline cells are considered to be functionally "immortal", both the germline and supporting somatic cells in the gonad within an organism will experience aging. With increased age at parenthood, the age-related decline in reproductive success has become an important biological issue for an aging population. However, molecular mechanisms underlying reproductive aging across sexes in vertebrates remain poorly understood. To decipher molecular drivers of vertebrate gonadal aging across sexes, we perform longitudinal characterization of the gonadal transcriptome throughout lifespan in the naturally short-lived African turquoise killifish *(Nothobranchius furzeri)*. By combining mRNA-seq and small RNA-seq from 26 individuals, we characterize the aging gonads of young adult, middle-aged, and old female and male fish. We analyze changes in transcriptional patterns of genes, transposable elements (TEs), and piRNAs. We find that testes seem to undergo only marginal changes during aging. In contrast, in middle-aged ovaries, the timepoint associated with peak female fertility in this strain, PIWI pathway components are transiently downregulated, TE transcription is elevated, and piRNA levels generally decrease, suggesting that egg quality may already be declining at middle-age. Furthermore, we show that piRNA ping-pong biogenesis declines steadily with age in ovaries, while it is maintained in aging testes. To our knowledge, this dataset represents the most comprehensive transcriptomic dataset for vertebrate gonadal aging. This resource also highlights important pathways that are regulated during reproductive aging in either ovaries or testes, which could ultimately be leveraged to help restore aspects of youthful reproductive function.

Introduction

In much of the industrialized world, parental age is increasing making fertility-related challenges associated with later-life childbearing increasingly relevant (Kenny et al. 2013; Bertoldo et al. 2020). In humans, oocyte quality begins to rapidly degrade around 30 years old while menopause, the irreversible loss of female fertility, occurs around 50 years old (Alberts et al. 2013; Finch 2014). In contrast, while male fertility gradually declines with age, complete loss of testicular function is not a feature of male reproductive aging (Gunes et al. 2016). Mammals, as well as birds, are exceptional among vertebrates as these groups produce a finite supply of oocytes before or shortly after birth ensuring that any species that lives long enough should eventually deplete its oocytes, although the starting supply of oocyte greatly outnumbers the final number of oocytes that will be ovulated (Mira 1998). However, there are many other mechanisms that influence reproductive decline, such as neuroendocrine aging, that occur in both sexes and are widely conserved among vertebrates (Perheentupa and Huhtaniemi 2009). Thus, leveraging a tractable vertebrate model organism to understand molecular mechanisms underlying reproductive aging will provide important insights into lifelong regulation of reproductive function.

To study reproductive aging, we examined the impact of aging on testes and ovaries in the African Turquoise Killifish *Nothobranchius furzeri*, the shortest-lived vertebrate that can be bred in captivity, with a lifespan of about 4-6 months (Hu and Brunet 2018). The turquoise killifish evolved this short lifespan in response to their unique lifecycle, which revolves around the formation of ephemeral ponds of water (Kim et al. 2016). Depending on the specific species, killifish can become sexually mature as early as two weeks post-hatching, although most killifish become sexually mature around 4-5 weeks of age, the fastest known time to sexual maturation of any vertebrate (Naumann and Englert 2018; Vrtilek et al. 2018b). Killifish are asynchronous breeders, and upon sexual maturity, females continuously undergo oogenesis and lay eggs, typically on a daily basis (Terzibasi Tozzini and Cellerino 2020). While male reproductive senescence may be negligible, females do experience an age-related decline in fecundity, though the molecular mechanisms

contributing to reproductive aging in either sex have not been elucidated (Vrtilek et al. 2018a; Zak and Reichard 2021). Importantly, we and others have helped establish a key functional genomics toolkit for this species, making it a uniquely tractable experimental model to decipher molecular mechanisms driving aspects of aging (Valenzano et al. 2011; Reichwald et al. 2015; Valenzano et al. 2015; Harel et al. 2016; Willemsen et al. 2020).

An emerging facet of vertebrate aging is the reactivation of transposable elements (TEs) with aging in somatic tissues (De Cecco et al. 2013; Chen et al. 2016; Simon et al. 2019; LaRocca et al. 2020; Yang et al. 2022). However, whether TEs also transcriptionally activate within the aging gonad, which is uniquely protected from spurious TE mobilization by the PIWI-piRNA pathway, has been largely unexplored in a vertebrate system. The PIWI pathway is an Argonaute-based small RNA pathway that maintains germline genomic integrity by antagonizing the mobilization of transposable elements (TEs) through complementary RNA base-pairing and TE RNA target degradation during gametogenesis and embryogenesis. PIWI family proteins bind 24-35 nucleotide (nt) PIWI-interacting RNAs, or piRNAs, which are complementary to or derived from TEs. piRNAs are expressed primarily in the gonad and are distinctly larger than miRNAs (Mani and Juliano 2013; Czech and Hannon 2016). Once bound to an RNA target, PIWI proteins cleave the RNA target precisely 10 nts from the 5' end of the complementary piRNA (Mani and Juliano 2013; Czech and Hannon 2016). To date, most studies examining the impact of aging on the PIWI pathway have focused on invertebrate model organisms, such as the fly *Drosophila melanogaster* (Sousa-Victor et al. 2017; Yamashiro and Siomi 2018; Lin et al. 2020). For instance, Piwi expression is required to suppress TE expression, reduce DNA damage, and maintain intestinal stem cell lineages in the aging Drosophila midgut (Sousa-Victor et al. 2017). In the fly ovary, age-related decline in *Piwi* expression in the cells of the germline stem cell niche results in a transposon de-repression and a loss of germline stem cells (GSCs) (Lin et al. 2020). In contrast to the germline stem cell niche, the expression of PIWI pathway components in whole *Drosophila* egg chambers increases with age, although this is not associated with any global changes in TE expression (Erwin and Blumenstiel 2019).

Whether TEs are derepressed with age in the vertebrate gonad and whether TE expression is modulated by age-related PIWI dynamics remains unknown. Thus, it will be important to determine whether PIWI regulation (and concomitant TE control) in the aging gonad may influence reproductive aging.

In this study, we leverage mRNA and small RNA sequencing to capture the transcriptional trajectory of gonadal aging in a naturally short-lived vertebrate. To do so, we characterize the transcriptome of African turquoise killifish ovaries and testes in young adults (5 weeks), middle-age (10 weeks) and old (15 weeks) animals in the GRZ inbred lab strain. In particular, we focus on the interplay of TEs and piRNAs, and assess the effect of age on the transcriptional status of these classes of RNAs.

Results

Lifespan, reproductive, and transcriptomic landscapes of the aging gonad in the African turquoise killifish

To understand how gonads are affected during aging in a vertebrate model organism, we performed a study of ovarian and testicular landscapes throughout aging in African turquoise killifish from the GRZ strain (**Fig. 1A**). In our housing conditions (see Methods), 15 weeks correspond to ~90% survival for both female and male animals (**Fig. 1B; Supplemental Table S1A**), although GRZ females lived significantly longer than males in our husbandry conditions ($p = 0.002$, log Rank test; see Methods) (**Fig. 1B**). To determine the effect of aging on the vertebrate gonadal transcriptomic landscape, we collected ovaries and testes from N = 5 GRZ female and male African turquoise killifish at three different time points post-hatching: young adulthood (5 weeks; onset of fertility), middle-age (10 weeks), and old age (15 weeks; before any dramatic population survival decrease) (**Fig. 1A**). The choice of these specific time points is consistent with broadly accepted guidelines in aging research, to avoid measuring development or survivorship bias (Flurkey et al. 2007) (see methods). In the highly inbred GRZ strain of African turquoise killifish, fecundity was reported to peak around 10-12 weeks of age (Zak and Reichard 2021), roughly corresponding to the middle-age time point that we selected. Only samples with intact RNA (RIN >7) were processed further to eliminate biases linked to RNA degradation, yielding 14 female samples and 12 male samples, leaving at least 4 samples per biological group (**Supplemental Fig. S1A**). We performed (i) mRNA transcriptome characterization (*i.e.* mRNA-seq using polyA selection), analyzing both transcriptional patterns of genes and transposable elements [TEs], and (ii) small-RNA transcriptome characterization (*i.e.* small RNA-seq), focusing on piRNAs, the germline-specific class of small RNAs of the PIWI pathway (**Fig. 1A** and **Supplemental Fig. S1A**).

To globally visualize the similarity of the transcriptomic landscapes of aging ovaries and testes at multiple levels of regulation, we used principal component analysis [PCA] (**Fig. 1C-E**). PCA analysis of genic mRNA, TE mRNA, and TE-targeting piRNA expression

revealed that the main source of variation [PC1] corresponded to gonadal identity (*i.e.* ovary vs. testis), although animal age also weakly separated samples for mRNA and piRNA cluster (but not TEs) transcription on PC2 (**Fig. 1C-E**). Notably, despite genomic TE content being a fixed feature for the species, we observed clear sex-dimorphism in the transcriptional landscape of TEs and associated piRNAs in the turquoise killifish gonads. These observations are consistent with deeply sex-dimorphic transcriptional programs in the gonad at the level of mRNAs, TEs and small RNAs, and are consistent with a recent study in young *Drosophila* ovaries and testes (Chen et al. 2021). Separately, we analyzed the ovarian and testicular transcriptomes to uncover potential sex-specific transcriptional patterns with aging (**Supplemental Fig. S1B-S**; see supplementary methods). Using PCA, we noted that middle-aged female expression data clustered distinctly for all analyzed RNA species in PC1 (**Supplemental Fig. S1B-D**). This observation may reflect the outsized contribution of a transcriptional program associated with oogenesis, or fertility more broadly, to the expression profiles of all RNA species assayed at this timepoint. Intriguingly, female piRNA expression data segregated most strongly by age, suggesting that the small RNA program in the ovary is most sensitive to aging (**Supplemental Fig. S1D**). In contrast, the male transcriptomic data did not visually separate strongly by age (**Supplemental Fig. S1E-G**).

Consistent with our PCA results, we noted stronger clustering of samples by age for ovaries compared to testes for gene, TE and piRNA expression using hierarchical clustering with bootstrap resampling by 'pvclust' (Suzuki and Shimodaira 2006) (**Supplemental Fig. S1H-M**; see supplementary methods). Finally, we also quantified the proportion of gene, TE and piRNA expression variance explained by age in the ovaries and testes using the 'variancePartition' framework (Hoffman and Schadt 2016) (**Supplemental Fig. S1N-S**; see supplementary methods). Importantly, the median percentage of variance explained by age was systematically higher in ovaries than testes (genes: ~25% *vs.* ~6%; TEs: ~15% *vs.* ~6; piRNAs: ~49% *vs.* ~2% ; **Supplemental Fig. S1N-S**). Together, our observations suggest that testicular identity and function are more stable in response to organismal aging relative to the ovary. Interestingly, our results are reminiscent of a microarray analysis of gonadal

aging in mice, where ovaries underwent substantially more transcriptional changes with aging than testes (Sharov et al. 2008). Our transcriptomic data is also consistent with observations of negligible male reproductive aging in this species (Vrtilek et al. 2018a; Zak and Reichard 2021). Together, our data suggests unique changes in the transcriptional landscapes of ovaries versus testes throughout aging.

Aging differentially impacts gene expression in turquoise killifish ovaries and testes

Since aging is often a non-linear process, at least in somatic tissues (Baumgart et al. 2016; Rosenberg et al. 2021), we decided to determine differential gene expression with aging within the DEseq2 framework using a likelihood ratio testing [LRT] approach, so as to unbiasedly identify patterns of differential gene expression in ovary and testis aging (Love et al. 2014). To note, since LRT can be overly lenient (Core 2021), we used a stringent False Discovery Rate [FDR] threshold of FDR <1e-6 to identify differentially expressed transcripts. Significantly regulated transcripts were then assigned to patterns using 'degPatterns' from the 'DEGreport' R package (Pantano 2022), which uses hierarchical clustering of gene expression to identify shared significant patterns of expression among differentially expressed genes in an unsupervised fashion. This unbiased approach detected four major differential patterns corresponding to transcripts whose expression is (a) transiently down at middle-age, (b) transiently up at middle-age, (c) monotonously down with age, or (d) monotonously up with age (**Fig. 2A-B**, **3A**, and **Supplemental Fig. S2A**, **S3A**; **Supplemental Table S2A-B,D**). For reading convenience, we label these age-related patterns of differential expression hereafter as (a), (b), (c) and (d) whenever they arise from the unsupervised 'degPatterns' clustering. Intriguingly, we noted the majority of differentially expressed genes showed transient changes at middle-age in both ovaries and testes (respectively 1931 out of 2041, and 578 out of 603 differentially expressed genes), rather than linear trends with age. This trend suggests that most of the transcriptional variation in gonadal gene expression occurs at middle-age when fertility, at least in females, is at its

peak. This observation is interesting, because it suggests that gonadal biology is already substantially impacted in middle-age healthy animals.

Next, we asked which biological functions were associated with each of these gene expression patterns with gonadal aging. For this purpose, we performed Gene Ontology [GO] Enrichment Analysis for each age-regulated pattern in ovaries and testes (Falcon and Gentleman 2007) (**Fig. 2C**, **3B**, and **Supplemental Fig. S2B, S3B**; **Supplemental Table S3A-F**). First, we examined enrichment for terms in the “Biological Process” GO category (**Fig. 2C**, **3B**; **Supplemental Table S3A,D**). Interestingly, genes downregulated in middle-aged ovaries were enriched most strongly for "piRNA metabolic process" (*i.e.* pattern a; GO:0034587; **Fig. 2C**; **Supplemental Table S3A**). Specifically, genes transcriptionally downregulated in middle-age ovaries include the genes encoding both effector PIWI proteins (*i.e.* the turquoise killifish homologs to human *PIWIL1* and *PIWIL2*), is consistent with overall decreased TE processing capacity. To note, as seen in **Supplemental Table S1C**, genes belonging to the “piRNA metabolic process” GO terms are, as expected, robustly expressed in killifish gonads throughout life.

Intriguingly, in zebrafish, the gene encoding PIWIL1, the primary catalytic protein of the PIWI pathway, is expressed most highly in developing germline stem cells before expression decreases in more mature oocytes (Liu et al. 2022), which could indicate a higher ratio of mature oocytes to developing germline stem cells in middle-aged killifish ovaries compared to young and old ovaries. Thus, downregulation of PIWI-related genes at mid-age may be related to differences in mature oocytes content. To test this hypothesis, we performed (i) a small-scale histological analysis of oocyte diameter in ovaries from fish at different ages (since oocyte size is directly linked to maturation) (Api et al. 2018) (**Supplemental Fig. S4A-B**; see supplementary methods), and (ii) used a bulk transcriptome deconvolution approach using a zebrafish single-cell RNA-seq dataset of young adult ovaries as a reference dataset (**Supplemental Fig. S4C-G**; see supplementary methods). First, histological analysis revealed that the diameter distribution of oocytes in aging African turquoise killifish ovaries, measured by 4 independent blinded observers, did not vary

218 significantly with age (**Supplemental Fig. S4B**). Second, whereas genes encoding PIWI-
219 related are sharply downregulated at middle-age, deconvolution analysis did not detect
220 substantial changes at middle-age in the proportion of immature germ cells in young *vs.*
221 middle-aged turquoise killifish ovaries (**Supplemental Fig. S4F,G**). Thus, it is unlikely that
222 observed bulk transcriptome changes in the expression of genes involved in piRNA
223 metabolism in the middle-aged killifish ovary reflect substantial changes in the underlying
224 ovarian composition of oocyte maturation stages. Alternatively, this may also suggest that
225 there is a relaxation of piRNA-mediated TE expression control in ovaries at middle-age in the
226 African turquoise killifish (see below). Other terms enriched for genes downregulated in
227 middle-age ovaries were largely related to egg maturation and egg-specific processes (*e.g.*
228 zona pellucida and regulation of acrosome reaction; **Fig. 2C**), consistent with the notion that
229 ovarian function (and oocyte quality) may have already started to decline at middle-age in
230 the African turquoise killifish.

231 Genes that were upregulated in middle-aged ovaries were enriched for terms related
232 to RNA metabolism, consistent with conserved importance of maternally deposited RNAs in
233 oocytes (*i.e.* pattern b; **Fig. 2C**). Genes that were linearly downregulated with age in the
234 ovaries were enriched for terms relating to extracellular matrix organization (*i.e.* pattern c;
235 **Fig. 2C**). Finally, genes that were upregulated with age in the ovaries included those
236 involved in immune responses and ion homeostasis (*i.e.* pattern d; **Fig. 2C**), which may
237 relate to overall increases in inflammation with aging that has been observed in somatic
238 tissues (Benayoun et al. 2019). Increased expression of inflammatory genes has also been
239 observed in the transcriptome of aging mouse ovaries (Sharov et al. 2008). We also
240 performed a similar functional enrichment analysis using terms from the "Cellular
241 Component" (**Supplemental Fig. S2B; Supplemental Table S3B**). and "Molecular
242 Function" (**Supplemental Table S3C**).GO categories, with largely consistent trends.

243 In aging testes, we observed the emergence of a similar trend, with most differential
244 genes being regulated at middle-age (*i.e.* patterns a and b), and few genes linearly regulated
245 with aging (*i.e.* patterns c and d; **Fig. 3A**; **Supplemental Table S3D**). Genes transiently

246 downregulated at middle-age were enriched for terms relating to vascular development
247 (pattern a; **Fig. 3B**). This observation suggests that the vasculature of the testis may be
248 actively remodeled, consistent with known unique vascular requirements for testicular
249 function (Sargent et al. 2015). Genes transiently upregulated at middle-age included those
250 involved in spermatogenesis, *e.g.* "axoneme assembly" and "cilium movement", consistent
251 with peak spermatogenesis potentially occurring at this stage (pattern b; **Fig. 3B**). Lastly,
252 genes that were downregulated linearly with age were heavily enriched for steroid
253 biosynthesis related terms, suggestive of a steady decline in steroid biosynthesis in the
254 aging gonad (pattern c; **Fig. 3B**). Interestingly, this transcriptional downregulation of steroid
255 biosynthesis genes is consistent with a recent mass-spectrometry study that detected
256 significantly decreased levels of sex-steroids in the testes of aging turquoise killifish
257 (Dabrowski et al. 2020). “Cellular component” analysis again corroborated the GO
258 “Biological Process” analysis, especially with regards to sperm-related terms being
259 upregulated at middle-age (**Supplemental Fig. S3B**; **Supplemental Table S3E**). Terms
260 downregulated at middle-age included those associated with heterochromatin and
261 extracellular vesicles, while terms downregulated linearly with age are enriched for
262 mitochondrial and collagen related terms (**Supplemental Fig. S3B**; **Supplemental Table**
263 **S3E**).

264 Together, our results show that the African turquoise killifish gonadal transcriptional
265 landscapes are broadly remodelled at middle-age, highlighting the need to include middle-
266 age time points in such analyses to get a full view of age-related trajectories. Notably, the
267 largest changes in gene expression seem to align with the window of peak fertility and egg
268 production in this species, suggesting that egg quality may start declining at middle-age
269 despite high egg output.

270

271 *Transposon expression is age- and sex-dependent in the turquoise killifish gonad*

272 Next, we asked whether control of TE transcription may be impacted during gonadal
273 aging in the turquoise killifish. Indeed, accumulating evidence has shown that TE expression

tends to increase with age in somatic tissues across species (De Cecco et al. 2013; Chen et al. 2016; Benayoun et al. 2019; Simon et al. 2019; Bravo et al. 2020; LaRocca et al. 2020; Yang et al. 2022). Although TE control is especially important in the germline to maintain genome stability throughout generations, whether TE expression escapes control in gonadal tissues with vertebrate aging has not yet been investigated. Interestingly, a recent genomic analysis of several species of African killifishes suggests that the shorter-lived killifish species have been accumulating TEs in their genomes, suggesting that short-lived/annual killifish species, such as the African turquoise killifish, may not efficiently repress germline TE activity throughout life (Cui et al. 2020).

To determine whether global changes in TE expression can indeed occur in aging killifish gonads, we first analyzed what proportion of mapped reads in our mRNA-seq dataset were derived from TE sequences (**Fig. 4A-B**). TE-derived sequences represented approximately 7-11% of reads in turquoise killifish ovaries and testes (**Fig. 4B**). Interestingly, global levels of TE-derived mRNA sequences were stable between young and middle-aged ovaries, but significantly dipped in old ovaries, whereas they tended to proportionally increase with age in testes (**Fig. 4B**). Such a pattern may reflect the process of gametogenesis, wherein the epigenome is repatterned, resulting in TE reactivation (Ben Maamar et al. 2021), despite the expected antagonizing effects of the PIWI pathway on TE expression in the germline.

Next, we asked whether TE transcription was changed with aging in ovaries and testes at the level of each subfamily. We identified differentially expressed TE transcripts using our mRNA-seq analysis pipeline (FDR < 1e-6, as above; **Fig. 4A,C,D** and **Supplemental Fig. S5A-B; Supplemental Table S4A-B**). Similar to our differential gene expression analysis, we observed that most significant changes in TE expression levels occurred in middle-aged gonads (*i.e.* patterns a and b; **Fig. 4C,D** and **Supplemental Fig. S5A,B**). In the ovary, 6 TEs were downregulated only at middle-age (pattern a), and 248 TEs were specifically upregulated at middle-age (pattern b; **Fig. 4C** and **Supplemental Fig. S5A**). These age-regulated TEs seem to belong to families broadly representative of the

overall turquoise killifish genomic TE content, with a predominance of LINE sequences, suggestive of general relaxation of TE control (**Fig. 4C,D**). Interestingly, this timepoint coincides with the functional enrichment for "piRNA metabolic process" for genes downregulated in middle-age ovaries (**Fig. 2C**). Thus, the transcriptional upregulation of TEs in the middle age ovary may reflect an unfavorable reactivation of certain TE species in response to the transient decline in PIWI pathway activity. Such an increase in TE transcription, even in the context of mature oocytes, is expected to be deleterious to oocyte health (Malki et al. 2014). No significant TEs were linearly downregulated or upregulated with age in the ovaries (*i.e.* patterns c and d, respectively; **Fig. 4C** and **Supplemental Fig. S5A**). In the aging testes, only 25 TEs passed our differential expression threshold (FDR < 1e-6), and they were all upregulated at middle-age (pattern b; **Fig. 4D** and **Supplemental Fig. S5B**). No significant TEs were downregulated at middle-age or linearly with age in the testes (*i.e.* patterns a, c, and d, respectively; **Fig. 4D** and **Supplemental Fig. S5B**). A burst of TE transcription in middle-age gonads could reflect peak fertility and gamete output, where a higher proportion of germ cells are undergoing epigenetic repatterning to yield increased numbers of mature gametes. Alternatively, increased TE transcription may reflect a relaxation of genome surveillance mechanisms, ultimately leading to decreased gamete quality and survivability.

piRNAs and the PIWI pathway activity are regulated throughout life in turquoise killifish gonads

Thus far, we have found that: (i) genes encoding the key components of the PIWI pathways are robustly expressed throughout life in turquoise killifish ovaries and testes (**Supplemental Table S1C**; **Fig. 5A**), (ii) PIWI pathway genes are downregulated in ovaries at middle-age (**Fig. 5A** and **2C**), and (iii) transcription of TEs is globally regulated with gonadal aging (**Fig. 4B**), with several TE subfamilies transcriptionally specifically upregulated in middle-age ovaries and, to a lesser extent, middle-age testes (**Fig. 4C,D**).

Thus, we reasoned that underlying changes in piRNA abundances throughout aging may drive changes in TE transcriptional levels.

To analyze PIWI pathway activity in ovaries and testes throughout turquoise killifish life, we generated small RNA sequencing libraries from the same samples used for mRNA-seq (**Fig. 1A**, **Supplemental Fig. S1A**). We leveraged these libraries to annotate piRNA clusters and evaluate piRNA expression throughout life in the African turquoise killifish gonads. First, to computationally isolate piRNAs from our small RNA-seq library, we used a size filter of 24-35 nucleotides, which was previously shown to efficiently capture piRNAs and separate them from miRNAs (Gong et al. 2018; Huang et al. 2019) (**Supplemental Fig. S6A**). Consistent with the resulting reads deriving from piRNAs, the resultant nucleotide composition showed the expected strong 1U bias in both types of gonads (Thomson and Lin 2009) (**Fig. 5B**). In addition, these piRNA-derived reads seemed to arise from 222 unique piRNA clusters in the turquoise killifish genome, as identified by Protrac (Rosenkranz and Zischler 2012). Importantly, the predicted TE content of the identified piRNA clusters is remarkably reflective of the annotated genomic TE content (**Fig. 5C**), consistent with the co-evolution between the TE invasion of the genome and the genomic defense against TE activity. In contrast to mice, in which ovarian piRNAs are rare and the PIWI pathway is broadly believed to be non-essential (Watanabe et al. 2008), turquoise killifish ovaries seem to express the components of PIWI pathway throughout life and are replete with piRNAs. This may be the result of continuous oocyte production in the killifish ovary since PIWI is required during oogenesis (Thomson and Lin 2009; Ketting 2011; Roovers et al. 2015).

Since piRNAs will align almost exclusively to TE sequences, we modelled piRNA abundance dynamics by performing differential expression analysis on TEs using counts from the piRNAs mapping to TE sequences embedded within the genome. This approach enables us to distinguish which TE species are differentially targeted by the PIWI pathway in turquoise killifish gonads as a function of age. As piRNA biogenesis is expected to at least partially be a response to TE activity, TE-specific piRNA counts should positively correlate with expressed TE species. Indeed, we observed a strong positive correlation between the

mRNA levels of TEs and the abundance of cognate piRNAs in each biological group (Spearman Rank correlation Rho ≥ 0.66; **Supplemental Fig. S6B,C**). Similar to transcriptional patterns observed in our genic and TE data, the bulk of differential piRNA expression occurred at middle-age in ovarian tissue (pattern a; **Fig. 5D** and **Supplemental Fig. S6D**; **Supplemental Table S5A**). However, mirroring the TE transcriptional changes where many TE species were upregulated in the middle-age ovaries (**Fig. 4C**), the majority of differentially abundant piRNAs were downregulated at middle-age in the ovaries (**Fig. 5D**), consistent with downregulation of the PIWI pathway genes (**Fig. 2C** and **5A**). Importantly, there was significant overlap between TEs that were specifically upregulated in middle-age ovaries and TEs targeted by piRNAs with decreased piRNA abundance in middle age ovaries ($p = 9.08E-3$ in Fisher's exact test; **Fig. 5F**), consistent with the notion of a partial relaxation of piRNA-mediated TE repression in middle-age ovaries. Testis piRNA expression was not as strongly regulated with age as compared to that of ovaries, with few age-regulated piRNA species, most of which showed increased expression with age (pattern d; **Fig. 5E** and **Supplemental Fig. S6E**).

Ping-Pong activity declines with age in oocytes, remains stable in testes

In the presence of a particular TE mRNA, the PIWI pathway initializes catalytic degradation of the TE transcript guided by TE-complementary "primary" piRNA sequences, which triggers the production of additional "secondary" piRNA sequences that specifically target the active TE sequence (Czech and Hannon 2016). This mechanism of piRNA synthesis through amplification of piRNA populations corresponding to actively transcribed TEs is known as "ping-pong" biogenesis (Czech and Hannon 2016) (**Fig. 6A**). Effectively, ping-pong biogenesis is an adaptive mechanism by which the PIWI pathway defends the germline against active TE threats (Czech and Hannon 2016). Due to the annealing requirements between primary piRNA sequences, target TE mRNAs, and TE-derived secondary piRNAs, a signature of ping-pong biogenesis is a 10 bp overlap between the 5' ends of opposite orientation piRNAs (Wang et al. 2015) (**Fig. 6A** and **Supplemental Fig.**

385 **S7A-B**). This ping-pong biogenesis mechanism can be measured globally or at the level of a
386 specific TE sequence.

387 We first used the PPmeter tool from the Protrac software suite to globally measure
388 ping-pong biogenesis rates in each biological group (Jehn et al. 2018) (**Fig. 6B**). This tool
389 calculates the instances of 10 bp overlaps out of every million overlap pairs assayed to
390 report the relative fraction of reads engaged in active ping-pong within a given piRNA
391 sequencing library. We used this tool for each biological replicate with 100 bootstraps and
392 report the median values in each biological sample over bootstrap samples (**Fig. 6B**). In
393 parallel, we also used an independent method in which, for each consensus TE sequence,
394 we computed Z_{10} scores, a standard measure of ping-pong activity defined as the Z-score of
395 the 10 bp overlap frequencies between opposite orientation piRNAs within a 20bp window
396 (Han et al. 2015; Vandewege et al. 2022). For each replicate, we took the median Z_{10} score
397 over all detected TE sequences to assess ping-pong at a global scale (**Fig. 6C**).
398 Convincingly, both orthogonal methods revealed a steady decrease of the piRNA population
399 participating in ping-pong biogenesis with aging in the ovaries, whereas this fraction
400 remained relatively stable in the testes (**Fig. 6C**). The age-related decline in ovarian ping-
401 pong activity may be related to a decrease in piRNA processing component expression
402 starting at middle age (**Fig. 5A**). This trend could result in a decrease in the ability of the
403 PIWI pathway to control TE transcription levels with ovarian aging. Alternatively, this steady
404 decrease with aging in ovarian ping-pong biogenesis may reflect the interplay of (i) a
405 decreased efficiency of the PIWI pathway at middle-age (**Fig. 2C**, **5A**), and (ii) an overall
406 decrease of TE transcription levels in old ovaries (**Fig. 4B**). Meanwhile, the observed steady
407 global ping-pong rates in testes are consistent with relatively stable TE and piRNA
408 expression dynamics relative to ovaries that we observed (**Fig. 4D, 5E**).

409 We were curious whether ping-pong biogenesis may be differentially regulated for
410 each consensus TE sequence. For this purpose, we further examined the consensus TE Z_{10}
411 data at the consensus TE transcript level. We used an ANOVA-based analysis to determine
412 which TEs have differential levels of ping-pong activity as measured by Z_{10} scores with aging

in ovaries and testes (**Fig. 6D-F** and **Supplemental Fig. S7C-D**). Then, TEs with significant age-related changes in ping-pong biogenesis were clustered into patterns, similar as before using the 'degPatterns' paradigm (**Fig. 2A**, **6D**). This analysis identified TEs with ping-pong biogenesis levels corresponding to previously described patterns b, c and d. In addition, it identified 2 significant patterns for TEs with decreased ping-pong biogenesis at middle-age (the pattern previously designated as (a)): (a_1) with maximal ping-pong biogenesis in the young gonad, or (a_2) maximal ping-pong biogenesis in the old gonad. Interestingly, most of the TEs showing differential ping-pong levels in the ovaries showed significantly decreased ping-pong with aging (pattern c; **Fig. 6E** and **Supplemental Fig. S7C**), consistent with the global ping-pong trends (**Fig. 6B,C**). In the testes, 82 TEs show differential ping-pong scores but without a clear global age-related trend, possibly reflecting a more robust PIWI activity throughout life (**Fig. 6F** and **Supplemental Fig. S7D**). In summary, multiple methods of analysis show ping-pong activity progressively wanes in the aging ovary, but remains steady in the testes which may be reflective of respective gametogenesis rates in the female versus male gonads throughout life.

Discussion

A resource for the study of reproductive aging in vertebrates

The germline is considered an immortal cell lineage but the somatic cells that comprise and support the germline are affected by aging. In this study, we examined how aging affects the female and male gonads of a naturally short-lived vertebrate species, the African turquoise killifish. To our knowledge, this dataset is the largest 'omic' dataset evaluating vertebrate ovarian and testicular aging and will represent a unique resource for reproductive aging research. To note, we performed this study using only fish from the inbred GRZ laboratory strain, a single genetic background of African turquoise killifish, continuously inbred since originally established in 1973. Thus, it is possible that other strains of this species may show different gonadal aging trajectories. For instance, other laboratory strains (*e.g.* MZM-0703, MZM-0410) are longer lived than the GRZ strain (Kim et al. 2016), and could thus exhibit differences in their reproductive aging patterns. Further, laboratory strains represent only a fraction of the genetic diversity available in the wild for this species. Indeed, GRZ and wild-derived turquoise killifish reared under the same laboratory conditions experience different fecundity and fertility rates during aging (Zak and Reichard 2021), although the same overall reproductive aging trends (albeit at different timescales) were observed across populations**.** Finally, African turquoise killifish may not experience significant age-related decline in reproductive function over their short lifespan in the wild, although a decline in relative fecundity (*i.e.* egg generation controlled for total body mass) has been reported in wild females (Vrtilek et al. 2018a). Thus, we note that future studies incorporating more genetically diverse strains (and in their natural habitat) may reveal variation in the patterns of molecular regulation of reproductive aging in this species.

With our inclusion of a middle-aged time point, in addition to young adult and old ages, this dataset enables the discovery of dynamic and non-linear patterns of regulation, thus helping understand gonadal aging trajectories in addition to just the endpoint of gonadal aging. Indeed, we found that many key events, including those relating to TE transcriptional regulation and piRNA pathway regulation, are most salient at middle-age in ovaries, rather

than undergoing linear changes with age. Our observations differ from reports in *Drosophila* egg chambers, in which PIWI-related genes were upregulated during aging though global TE expression levels remained largely stable (Erwin and Blumenstiel 2019). Importantly, our observations that the aging ovarian transcriptome is more impacted than the testicular transcriptome are consistent with previous microarray studies of mouse gonadal aging (Sharov et al. 2008). To note, in long-lived species (*e.g.* humans), male germ cells can accumulate mutations from repeated divisions during aging, which can impact offspring fitness and disease risk – the "father's age effect" (Kong et al. 2012). Due to the relatively short lifespan of vertebrate models used in aging research (*i.e.* African turquoise killifish, mouse), it is unlikely that the impact of repeated male germ cell divisions over male lifespan can be appropriately modeled in these species, thus potentially explaining the relative paucity of changes observed in the molecular landscapes of aging testes.

A unique crosstalk between piRNA biogenesis and TE activity in the aging vertebrate gonad

We characterized TE expression and PIWI pathway behavior throughout life in turquoise killifish ovaries and testes. Importantly, we found that the PIWI pathway controls TE expression in the gonads throughout the turquoise killifish lifespan. Age-related fertility decline is common across many metazoans (Jones et al. 2014). The turquoise killifish is no exception to this rule, with fertility generally declining after middle-age, especially in females (Zak and Reichard 2021). For both sexes, fertility peaks around the middle-age timepoint used in this study (Zak and Reichard 2021). Interestingly, this timepoint coincided with the largest changes in TE- and piRNA related events in both sexes, albeit much more pronounced in ovaries compared to testes. This may correspond to a period of increasing gametogenesis in which epigenetic modifications are globally removed from germ cells prior to repatterning. Such epigenetic erasure would provide a means of "escape" for TEs in the form of transcription. Since the females are asynchronous spawners and continuously produce oocytes, we might expect that, like in males, TE transcription may reflect gamete production output. To note, our observations may capture differential amplitudes of

reproductive aging between the sexes - with more dramatic increases in TE transcription in ovaries, which undergo a clearly measurable reproductive senescence, compared to more modest changes in testes, which are thought to undergo near negligible reproductive senescence (Vrtilek et al. 2018a; Zak and Reichard 2021).

Overall, even in this short-lived species, the PIWI pathway seems to broadly keep gonadal TE transcription stable at the global transcriptomic level (**Fig. 4B**), although there is clear regulatory variation depending on specific TE sequences. This relatively controlled transcriptional output for TE loci seems to contrast with reports of global transcriptional derepression of TE sequences in aging somatic tissues (De Cecco et al. 2013; Bravo et al. 2020). When expressed, TEs can cause DNA damage and/or initiate innate immune responses due to their intrinsic similarity to viruses (Simon et al. 2019). This contrast between TE activity in germline/somatic tissues is especially interesting considering that non-aging taxa (*e.g. Hydra*, *Planaria*) can express PIWI in somatic stem cells (Schaible et al. 2015; Sahu et al. 2017; Teefy et al. 2020). This suggests that looser TE control may drive aspects of aging, especially in the soma, whereas tighter TE control is crucial to allow the emergence of non-aging states, such as those found in the germline.

Dynamic TE control in the aging African turquoise killifish ovary

If piRNA metabolism dynamics in the turquoise killifish ovary are similar to those of zebrafish (with *PIWIL1* expression being largely confined to immature germ cells) (Liu et al. 2022), then downregulation of PIWI-related genes in bulk middle-age ovaries could merely reflect a lower underlying proportion of immature oocytes. However, our histological and deconvolution analyses suggest that large scale changes in oocytes maturation are unlikely to underlie observed changes in PIWI pathway activity during ovarian aging (**Supplemental Fig. S4**).

Alternatively, increased TE expression in middle-aged ovaries (and thus decreased TE control) may be a symptom of decreased oocyte quality before fertility starts to decline, suggesting that reproductive aging may precede organismal decline. Specifically, decreased

514 TE transcription and increased expression of PIWI pathway components in old ovaries may
515 constitute a delayed response to increased TE transcription and decreased expression of
516 PIWI pathway components at middle-age.

517 Finally, it is possible that such a transient relaxation of TE control in middle-age
518 ovaries for the turquoise killifish may have adaptative value. Indeed, parental age in the
519 turquoise killifish has been proposed to convey environmental information for evolutionary
520 benefit. Embryos of old breeders enter are more likely to state of suspended animation
521 known as diapause, which killifish utilize to persist under dry conditions between rainy
522 seasons, than the embryos of young breeders (Api et al. 2018). Within a single wet season,
523 the offspring of older mothers are more likely to immediately encounter a dry season, while
524 those of younger mothers are more likely to propagate and yield multiple generations (Api et
525 al. 2018).

526 Likewise, allowing some level of age-associated TE mobilization in the germline
527 through tunable activity of the PIWI pathway could help ensure adequate levels of genetic
528 diversity in a species with naturally small populations due to its unique ecology. Consistently,
529 annual killifish, like *Nothobranchius furzeri*, have much higher genomic TE content than non-
530 annual killifish species that do not experience such extreme population bottlenecks from
531 seasonal aquatic habitat desiccation (Cui et al. 2020). TEs have long been appreciated in
532 plant biology for their contribution to genetic diversity and are now appreciated sources of
533 genetic diversity and drivers of speciation in animals (McClintock 1984; Gonzalez et al.
534 2010; Akagi et al. 2013; Belyayev 2014; Bariah et al. 2020; Chen et al. 2020; Catlin and
535 Josephs 2022). In line with the hypothesis that relaxed germline TE restriction may enhance
536 population-level genetic diversity is our observation that ping-pong rate in killifish ovaries
537 decreases steadily with age. This age-related PIWI behavior could support a population
538 facing severe bottlenecks by first generating many healthier (but less genetically diverse)
539 progeny during young adulthood. Subsequently, with females still breeding at a more
540 advanced age, reduced PIWI pathway activity could help generate a more genetically

diverse pool of progeny that could improve genetic diversity for the long-term adaptability of the local population.

In summary, our data supports the notion that even a short-lived species such as the African turquoise killifish can maintain adequate TE silencing in germline-containing tissues throughout life, likely due to the activity of the PIWI pathway. The impact of fluctuations in TE transcription and PIWI pathway activity, especially in ovarian tissues, remains an open question. Understanding disruptions to gonadal genomic regulatory networks during aging will be crucial to define strategies to preserve or prolong reproductive fitness with aging.

Material and methods

African turquoise killifish husbandry

African turquoise killifish were raised according to gold standard procedures (Dodzian et al. 2018). To decrease risks of aggression, adult fish were single housed in 2.8L tanks on a recirculating aquatics system manufactured by Aquaneering Inc. System water parameters were as follows: temperature: 29°C; pH: 7.3; conductance: 670-750 µS; ammonia and nitrite: 0ppm and Nitrate: ~15 ppm. Adult fish were fed twice per day with Hikari Freeze Dried Bloodworms 4-6 hours apart, and live *Artemia* once per day. Fry were reared in system water incubated at 28°C, then placed on the recirculating system starting at 2 weeks post hatch. Fry were fed live *Artemia* exclusively until 4 weeks post hatch. The fish facility was kept on a light/dark cycle of 13/11 hours (lights on 9am-10pm). The fish were euthanized by immersion in 1.5 g/L of Tricaine MS-222 dissolved in system water followed by decapitation. All fish were euthanized between 2 and 4 pm to minimize circadian effects. All husbandry conditions and experimental procedures were approved by the University of Southern California (USC) IACUC. Animal care and animal experimentation were performed in accordance with IACUC approved protocols for *Nothobranchius furzeri at* the University of Southern California (approved protocols *20879* and *21023*).

Lifespan data collection

Lifespan data was derived from historical data in our colony collected 2019-2022. Time from hatching to humane endpoint/euthanasia or natural death was recorded as killifish lifespan. All lifespan data reported here is derived from single-housed fish to limit death or injuries linked with frequent fighting in this species.

RNA extraction and sequencing

Ovaries and testes were dissected from 5-week-old, 10-week-old, and 15-week-old turquoise killifish (N = 5 per group) and flash-frozen on dry ice. Our chosen number of biological replicates for each group is in the range shown to be robust for differential gene

expression analysis by RNA-seq (Lamarre et al. 2018). Importantly, we defined the 3 age groups based on generally accepted guidelines in the field of aging research: (i) the chosen "young" adult time point at 5 weeks represents sexual maturity (*i.e.* the age at which individuals are able to reproduce), to avoid measuring developmental signals, (ii) the chosen "old" time point at 15 weeks represents ~90% population survival in our GRZ colony regardless of sex (**Fig. 1B**), allowing sample of aged animals before any risk of survivorship bias (Flurkey et al. 2007), and (iii) the chosen "middle-aged" time point at 10 weeks is the midpoint between these extremes. Total RNA was extracted from flash-frozen gonads by homogenizing using Trizol (Thermo Fisher, 15596018) and Lysing Matrix D tubes (MP Biomedicals, 11422420) on a BeadBug 6 microtube homogenizer (Millipore Sigma, Z742683) for 2 rounds of 30 seconds at 3500 rpms. RNA was assayed for quality at the USC Genome Core using the Agilent Bioanalyzer total RNA assay, and only high-quality RNA samples (RIN > 7) were selected for further processing to avoid RNA degradation related biases. Due to poor RNA quality, samples for three males (one from each age group) and one 15-week female were eliminated at this stage. RNA samples were sent to Novogene Corporation (USA) for library construction and sequencing, where mRNA and small RNA sequencing libraries were generated from the same total RNA samples in parallel. mRNA libraries were prepared by enrichment with oligo(dT) beads and sequenced on an Illumina NovaSeq 6000 generating 150 bp paired-end libraries. Small RNA seq libraries were generated by 3' adapter ligation, 5' adapter ligation, reverse transcription, PCR amplification, and gel purification and size selection. Small RNA samples were sequenced on an Illumina Novaseq 6000 generating 50 nucleotide single-end read libraries. Raw sequencing data has been deposited to SRA under PRJNA854614.

mRNA-seq data pre-processing and genomic alignment

FASTQ reads from mRNA libraries were first hard-trimmed using fastx_trimmer (fastx_toolkit 0.0.13) (Gordon A. 2010), to remove 5' adapter fragments and low quality bases at the 3' end of the reads using parameters "-f 16", "-l 100", and "-Q33". Next, Illumina

adapters were removed using TrimGalore 0.6.7 (cutadapt 3.3) (Felix Krueger 2021). To maximize our capture of relevant reads, we used the most contiguous genome reference currently available for the African turquoise killifish, Genbank accession GCA_014300015.1, described in Williamsen *et al.,* 2020 (Willemsen et al. 2020), as well as its corresponding gene annotation file. Since analysis of repetitive sequences was desired, we performed soft-masking with Repeatmasker 4.1.2-p1 (Smit 2013-2015) and a turquoise killifish specific consensus TE library downloaded from FishTEDB (downloaded: February 5, 2021) (Shao et al. 2018). A TE-specific GTF file for downstream analysis was generated using a custom R script for compatibility with the TETranscripts counting program (Jin et al. 2015). RNA-seq reads were aligned to the soft-masked turquoise killifish genome using STAR 2.7.0e, allowing 200 multimappers to accommodate TE sequence alignment (Dobin et al. 2013; Jin et al. 2015). Gene and TE counts were generated using TETranscripts 2.2.1 with default settings using gene annotations from GenBank and the RepeatMasker derived custom TE-specific GTF file.

Differential gene and TE expression analysis

The TETranscripts count matrices for genes and TEs were analyzed together in R 4.1.2 using DESeq2 v1.34.0 (Love et al. 2014). To identify differentially expressed transcripts and their patterns with aging in ovaries and testes, we used likelihood ratio testing [LRT] separately for each sex with each age as its own group. Significant genes were defined as those with an adjusted p-value of < 1E-6 with the DESeq2 LRT test. Genes and TEs were then analyzed separately. Once significantly differentially expressed genes and TEs were identified, clusters of differentially expressed genes and TEs were unbiasedly identified using the 'degPatterns' function from the 'DEGreport' v1.30.3 package (Pantano 2022).

Fractional TE analysis

633 To compare fractional TE expression in killifish gonads, the TEtranscripts count
634 matrices used for differential gene and TE expression analysis were imported into R. For
635 each biological replicate, assigned counts were classified as genic or TE-derived and the
636 fractional TE representation for each replicate library was calculated as TE read counts
637 divided by total read counts. Fractional counts were grouped by age and sex and tested for
638 significance by the non-parametric Wilcoxon rank sum test between groups within each sex.
639
640 *Functional enrichment analysis*
641 Data was prepared for functional enrichment analysis by running blastp (ncbi-blast
642 v2.13.0) with African turquoise killifish protein sequences from the (Willemsen, 2020)
643 GCA_014300015.1 genome version, against Ensembl release 104 human protein
644 sequences. For each query killifish sequence, only top hits with E-value < 1e-3 were
645 retained, and these human homologs were used for functional enrichment analyses. Gene
646 ontology (GO) enrichment analysis was performed using 'GOstats' 2.60.0 with GO terms
647 downloaded using 'biomaRt' 2.50.3 (Durinck et al. 2009) corresponding to Ensembl release
648 104. GO analysis was performed using the "Biological Process", "Cellular Component", and
649 "Molecular Function" categories with a significance threshold equal to a false discovery rate
650 [FDR] < 5%. GO analysis was performed on each of the gene patterns identified in the LRT-
651 based DGE analysis described above.
652
653 *piRNA selection, annotation, and piRNA cluster analyses*
654 FASTQ reads from small RNA libraries were trimmed of their adapters while keeping
655 a minial length of at least 18 nucleotides using TrimGalore 0.6.7 (cutadapt 3.3) (Felix
656 Krueger 2021) with the commands "--length 18", "-a
657 GTTCAGAGTTCTACAGTCCGACGATC", and "-a GTTCAGAGTTCTACAGTCCGACGATC".
658 piRNAs were selected by size-selecting sequences between 24-35 nucleotides in length
659 from the trimmed small RNA libraries (Gong et al. 2018; Huang et al. 2019). piRNA length
660 distributions (**Supplemental Fig. S6A**) were generated by combining piRNA length

661 histogram data by sex and plotting the resultant length distribution in R. piRNA nucleotide
662 distribution for each sex was computed by converting piRNA reads to fasta format files and
663 concatenating by sex. Position weight matrices were generated from these fasta files in R
664 using the package 'Biostrings' 2.58.0 (**Fig. 5B**). Sequence logos were generated from
665 position weight matrices using the R package 'ggseqlogo' 0.1.

666 To identify piRNA clusters, we used the Protrac 2.42 software suite (Rosenkranz and
667 Zischler 2012). Briefly, piRNAs were collapsed to unique reads, while retaining count
668 numbers using the functions TBr2_collapse.pl and TBr2_duster.pl. These reads were then
669 mapped to the soft-masked reference genome described previously using the function
670 sRNAmapper.pl and clusters were identified by a preponderance of piRNA mapping within a
671 particular window using the function proTRAC_2.4.3.pl. Clusters were identified for each
672 biological replicate before being combined such that only unique piRNA clusters remained
673 using the Protrac function merge.pl. To assess the TE composition of piRNA clusters relative
674 to the genome, the intersectbed command (bedtools 2.27.1) was used to extract piRNA
675 cluster fasta sequences from the genome (Quinlan and Hall 2010). Then, Repeatmasker
676 4.1.2-p1 was run as above on the isolated piRNA cluster fasta sequences to obtain TE
677 family information, which was then contrasted with the genome-wide data in R.

678

679 *piRNA differential expression and Ping-Pong analysis*

680 piRNAs were mapped to the soft-masked genome reference using bowtie 1.2.3
681 (Langmead et al. 2009) with three allowed mismatches since piRNAs are known to bind with
682 imperfect base-pairing (Juliano et al. 2014; George et al. 2015; Zhang et al. 2015; Teefy et
683 al. 2020) using the parameters "-v 3 -a --best --strata -S" before being converted to bam
684 format files with samtools 1.10 (Danecek et al. 2021). piRNA counts were then assigned
685 using 'featureCounts' from the Subread 2.0.2 package, using fractional count attribution for
686 multimapping reads (Liao et al. 2014). For featureCounts based read counting, a custom
687 GTF file consisting of genes, TEs, piRNA clusters, and rRNA repeats as features was used
688 to account for piRNA mapping to all relevant features to minimize biases in piRNA counts.

The resultant count matrix was imported into R, and rRNA-mapping reads were discarded prior to normalization. Then piRNA counts that mapped to genes, TEs, and piRNA clusters were normalized together using DEseq2. LRT-based clustering and DGE analysis was then performed for piRNA counts that mapped to TE sequences as described above.

To measure ping-pong biogenesis, we only considered piRNAs mapping to consensus TE sequences, since they constitute the most biologically relevant target of gonadal piRNAs. To analyze ping-pong biogenesis at a global level, we used the PPmeter 0.4 program (Jehn et al. 2018). Briefly, PPmeter reports the rate of 10 bp overlaps between piRNA reads, a proxy for ping-pong biogenesis, by generating pseudo-replicates through boostrapping one million piRNA reads (100 bootstraps). Using this approach, piRNA libraries can be directly compared to each other by measuring the number of ping-pong events (*i.e.* 10 bp overlaps) per one million piRNA reads. The resultant metric, ping-pong rate per million bootstrapped reads (ppr-mbr) was calculated for each bootstrap in each piRNA library. Bootstrap values were combined per biological replicate and the median value was taken. Median ppr-mbr values were then grouped by age and sex and tested for statistical difference by age group within each sex by the non-parametric Wilcoxon rank sum test.

For TE-specific level ping-pong measurement, we used custom scripts that calculated Z_{10} scores for each consensus TE sequence. Z_{10} scores, as defined in (Han et al. 2015; Vandewege et al. 2022) is the difference of 10 bp overlap occurrences and the mean of all other overlap occurrences within a 20 bp window divided by the standard deviation of all other overlap occurrences. This is shown in the following equation:

$$Z_{10} = \frac{(10\ bp\ overlaps) - (\mu_{1:9,11:20\ bp}\ overlaps)}{\sigma_{1:9,11:20\ bp}\ overlaps}$$

To generate Z_{10} scores, the distances between piRNA 5' ends that mapped to opposite strands of consensus TE sequences were tabulated into a histogram using a custom bash script. The resultant histograms were imported into R and processed in a

715 custom script that reported the Z_{10} score for each consensus TE sequence. For some TE
716 sequences, coverage was incomplete such that we could not derive Z_{10}-score information;
717 these sequences were discarded from consideration. To measure the changes in Z_{10} scores
718 with age, TE Z_{10} scores were separated by sex and grouped by age. Group-level Z_{10} scores
719 were tested for significant differences by 1-way ANOVA in R, and only TEs with an adjusted
720 p-value <0.05 were considered significantly regulated with aging in either gonad type.
721 Significant TEs were then classified into clusters using the 'degPatterns' function from
722 'DEGreport' 1.30.3 package as described previously. For biological group-level analysis of
723 Z_{10} scores, median Z_{10} values over all detected TE sequences were taken for each biological
724 replicate and plotted as a function of age and sex. Difference in Z_{10} scores per group were
725 tested between age groups within sexes by a non-parametric Wilcoxon rank sum test.
726
727 *Scripts and code availability*
728 All scripts used in this study are available as an archive accompanying this
729 manuscript (Supplemental Code), and on the Benayoun laboratory Github
730 (https://github.com/BenayounLaboratory/Killifish_reproductive_aging_resource). All R scripts
731 were run using R version 4.1.2.
732
733
734 **Data access**
735 All raw sequencing data generated in this study have been submitted to the NCBI
736 BioProject database (https://www.ncbi.nlm.nih.gov/bioproject/) under accession number
737 PRJNA854614.
738
739

Competing interest statement

The authors have no conflict of interest.

Acknowledgments

Some panels were made with BioRender.com. We thank Suchi Patel of the USC Genome Core for running RNA bioanalyzer assays. We thank Jomille Jerez, Isabel Ollerton, Rajyk Bhala and Katelyn Hsu for assistance with killifish husbandry. We thank Dr. Carolyn Phillips, Dr. Minhoo Kim, Dr. Itamar Harel, Justin Gilmore, Juan Bravo, Casandra McGill, and Rajyk Bhala for insights and feedback on our manuscript. We thank Drs. Ryo Sanabria and Gilberto Garcia for advice on histological image analysis using ImageJ. This work was supported by an NIA T32 AG052374 Postdoctoral Training Grant fellowship to B.B.T, NIA R21 AG063739, NIGMS R35 GM142395, a pilot grant from the NAVIGAGE Foundation, and a Hanson-Thorell Family award to B.A.B.

The authors acknowledge the Center for Advanced Research Computing (CARC) at the University of Southern California for providing computing resources that have contributed to the research results reported within this publication (https://carc.usc.edu). Ovarian histological analysis was performed by the Translational Pathology Core at the USC Norris Comprehensive Cancer Center (supported by NCI P30 CA014089).

Author contributions

B.B.T. and B.A.B. designed the study. B.B.T. and A.A. performed fish husbandry. A.A. dissected killifish gonadal tissues. B.B.T. performed RNA extraction of samples and computational analyses, with assistance from A.X., P.P.S. and B.A.B. B.B.T. and B.A.B. wrote the manuscript with input from all authors. K.H. captured microscope images of aging ovaries, B.B.T., A.X., K.H. and B.A.B. conducted ImageJ analysis of ovarian histology. All authors edited and commented on the manuscript.

References

Akagi K, Li J, Symer DE. 2013. How do mammalian transposons induce genetic variation? A conceptual framework: the age, structure, allele frequency, and genome context of transposable elements may define their wide-ranging biological impacts. *Bioessays* **35**: 397-407.

Alberts SC, Altmann J, Brockman DK, Cords M, Fedigan LM, Pusey A, Stoinski TS, Strier KB, Morris WF, Bronikowski AM. 2013. Reproductive aging patterns in primates reveal that humans are distinct. *Proc Natl Acad Sci U S A* **110**: 13440-13445.

Api M, Notarstefano V, Olivotto I, Cellerino A, Carnevali O. 2018. Breeders Age Affects Reproductive Success in Nothobranchius furzeri. *Zebrafish* **15**: 546-557.

Bariah I, Keidar-Friedman D, Kashkush K. 2020. Where the Wild Things Are: Transposable Elements as Drivers of Structural and Functional Variations in the Wheat Genome. *Front Plant Sci* **11**: 585515.

Baumgart M, Priebe S, Groth M, Hartmann N, Menzel U, Pandolfini L, Koch P, Felder M, Ristow M, Englert C et al. 2016. Longitudinal RNA-Seq Analysis of Vertebrate Aging Identifies Mitochondrial Complex I as a Small-Molecule-Sensitive Modifier of Lifespan. *Cell Syst* **2**: 122-132.

Belyayev A. 2014. Bursts of transposable elements as an evolutionary driving force. *J Evol Biol* **27**: 2573-2584.

Ben Maamar M, Nilsson EE, Skinner MK. 2021. Epigenetic transgenerational inheritance, gametogenesis and germline developmentdagger. *Biol Reprod* **105**: 570-592.

Benayoun BA, Pollina EA, Singh PP, Mahmoudi S, Harel I, Casey KM, Dulken BW, Kundaje A, Brunet A. 2019. Remodeling of epigenome and transcriptome landscapes with aging

in mice reveals widespread induction of inflammatory responses. *Genome Res* **29**: 697-709.

Bertoldo MJ, Listijono DR, Ho WJ, Riepsamen AH, Goss DM, Richani D, Jin XL, Mahbub S, Campbell JM, Habibalahi A et al. 2020. NAD(+) Repletion Rescues Female Fertility during Reproductive Aging. *Cell Rep* **30**: 1670-1681 e1677.

Bravo JI, Nozownik S, Danthi PS, Benayoun BA. 2020. Transposable elements, circular RNAs and mitochondrial transcription in age-related genomic regulation. *Development* **147**.

Catlin NS, Josephs EB. 2022. The important contribution of transposable elements to phenotypic variation and evolution. *Curr Opin Plant Biol* **65**: 102140.

Chen H, Zheng X, Xiao D, Zheng Y. 2016. Age-associated de-repression of retrotransposons in the Drosophila fat body, its potential cause and consequence. *Aging Cell* **15**: 542-552.

Chen J, Lu L, Robb SMC, Collin M, Okumoto Y, Stajich JE, Wessler SR. 2020. Genomic diversity generated by a transposable element burst in a rice recombinant inbred population. *Proc Natl Acad Sci U S A* **117**: 26288-26297.

Chen P, Kotov AA, Godneeva BK, Bazylev SS, Olenina LV, Aravin AA. 2021. piRNA-mediated gene regulation and adaptation to sex-specific transposon expression in D. melanogaster male germline. *Genes Dev* **35**: 914-935.

Core HCB. 2021. DGE analysis using LRT in DESeq2. Vol 2022.

Cui R, Medeiros T, Willemsen D, Iasi LNM, Collier GE, Graef M, Reichard M, Valenzano DR. 2020. Relaxed Selection Limits Lifespan by Increasing Mutation Load. *Cell* **180**: 1272-1279.

814 Czech B, Hannon GJ. 2016. One Loop to Rule Them All: The Ping-Pong Cycle and piRNA-
815 Guided Silencing. *Trends Biochem Sci* **41**: 324-337.
816 Dabrowski R, Ripa R, Latza C, Annibal A, Antebi A. 2020. Optimization of mass spectrometry
817 settings for steroidomic analysis in young and old killifish. *Anal Bioanal Chem* **412**:
818 4089-4099.
819 Danecek P, Bonfield JK, Liddle J, Marshall J, Ohan V, Pollard MO, Whitwham A, Keane T,
820 McCarthy SA, Davies RM et al. 2021. Twelve years of SAMtools and BCFtools.
821 *Gigascience* **10**.
822 De Cecco M, Criscione SW, Peterson AL, Neretti N, Sedivy JM, Kreiling JA. 2013.
823 Transposable elements become active and mobile in the genomes of aging
824 mammalian somatic tissues. *Aging (Albany NY)* **5**: 867-883.
825 Dobin A, Davis CA, Schlesinger F, Drenkow J, Zaleski C, Jha S, Batut P, Chaisson M, Gingeras
826 TR. 2013. STAR: ultrafast universal RNA-seq aligner. *Bioinformatics* **29**: 15-21.
827 Dodzian J, Kean S, Seidel J, Valenzano DR. 2018. A Protocol for Laboratory Housing of
828 Turquoise Killifish (Nothobranchius furzeri). *J Vis Exp* doi:10.3791/57073.
829 Durinck S, Spellman PT, Birney E, Huber W. 2009. Mapping identifiers for the integration of
830 genomic datasets with the R/Bioconductor package biomaRt. *Nat Protoc* **4**: 1184-
831 1191.
832 Erwin AA, Blumenstiel JP. 2019. Aging in the Drosophila ovary: contrasting changes in the
833 expression of the piRNA machinery and mitochondria but no global release of
834 transposable elements. *BMC Genomics* **20**: 305.
835 Falcon S, Gentleman R. 2007. Using GOstats to test gene lists for GO term association.
836 *Bioinformatics* **23**: 257-258.

837 Felix Krueger FJ, Phil Ewels, Ebrahim Afyounian, & Benjamin Schuster-Boeckler. 2021.
838 FelixKrueger/TrimGalore: v0.6.7 - DOI via Zenodo (0.6.7). Zenodo.
839 https://doi.org/10.5281/zenodo.5127899. Accessed August 20, 2021.
840 Finch CE. 2014. The menopause and aging, a comparative perspective. *J Steroid Biochem*
841 *Mol Biol* **142**: 132-141.
842 Flurkey K, Currer J, Harrison D. 2007. The Mouse in Aging Research. *The Mouse in*
843 *Biomedical Research* **3**.
844 George P, Jensen S, Pogorelcnik R, Lee J, Xing Y, Brasset E, Vaury C, Sharakhov IV. 2015.
845 Increased production of piRNAs from euchromatic clusters and genes in Anopheles
846 gambiae compared with Drosophila melanogaster. *Epigenetics Chromatin* **8**: 50.
847 Gong J, Zhang Q, Wang Q, Ma Y, Du J, Zhang Y, Zhao X. 2018. Identification and verification
848 of potential piRNAs from domesticated yak testis. *Reproduction* **155**: 117-127.
849 Gonzalez J, Karasov TL, Messer PW, Petrov DA. 2010. Genome-wide patterns of adaptation
850 to temperate environments associated with transposable elements in Drosophila.
851 *PLoS Genet* **6**: e1000905.
852 Gordon A. HG. 2010. FASTX-Toolkit. *Unpublished*.
853 Gunes S, Hekim GN, Arslan MA, Asci R. 2016. Effects of aging on the male reproductive
854 system. *J Assist Reprod Genet* **33**: 441-454.
855 Han BW, Wang W, Li C, Weng Z, Zamore PD. 2015. Noncoding RNA. piRNA-guided
856 transposon cleavage initiates Zucchini-dependent, phased piRNA production. *Science*
857 **348**: 817-821.
858 Harel I, Valenzano DR, Brunet A. 2016. Efficient genome engineering approaches for the
859 short-lived African turquoise killifish. *Nat Protoc* **11**: 2010-2028.

Hoffman GE, Schadt EE. 2016. variancePartition: interpreting drivers of variation in complex gene expression studies. *BMC Bioinformatics* **17**: 483.

Hu CK, Brunet A. 2018. The African turquoise killifish: A research organism to study vertebrate aging and diapause. *Aging Cell* **17**: e12757.

Huang S, Ichikawa Y, Igarashi Y, Yoshitake K, Kinoshita S, Omori F, Maeyama K, Nagai K, Watabe S, Asakawa S. 2019. Piwi-interacting RNA (piRNA) expression patterns in pearl oyster (Pinctada fucata) somatic tissues. *Sci Rep* **9**: 247.

Jehn J, Gebert D, Pipilescu F, Stern S, Kiefer JST, Hewel C, Rosenkranz D. 2018. PIWI genes and piRNAs are ubiquitously expressed in mollusks and show patterns of lineage-specific adaptation. *Commun Biol* **1**: 137.

Jin Y, Tam OH, Paniagua E, Hammell M. 2015. TEtranscripts: a package for including transposable elements in differential expression analysis of RNA-seq datasets. *Bioinformatics* **31**: 3593-3599.

Jones OR, Scheuerlein A, Salguero-Gomez R, Camarda CG, Schaible R, Casper BB, Dahlgren JP, Ehrlen J, Garcia MB, Menges ES et al. 2014. Diversity of ageing across the tree of life. *Nature* **505**: 169-173.

Juliano CE, Reich A, Liu N, Gotzfried J, Zhong M, Uman S, Reenan RA, Wessel GM, Steele RE, Lin H. 2014. PIWI proteins and PIWI-interacting RNAs function in Hydra somatic stem cells. *Proc Natl Acad Sci U S A* **111**: 337-342.

Kenny LC, Lavender T, McNamee R, O'Neill SM, Mills T, Khashan AS. 2013. Advanced maternal age and adverse pregnancy outcome: evidence from a large contemporary cohort. *PLoS One* **8**: e56583.

Ketting RF. 2011. The many faces of RNAi. *Dev Cell* **20**: 148-161.

883 Kim Y, Nam HG, Valenzano DR. 2016. The short-lived African turquoise killifish: an emerging
884 experimental model for ageing. *Dis Model Mech* **9**: 115-129.
885 Kong A, Frigge ML, Masson G, Besenbacher S, Sulem P, Magnusson G, Gudjonsson SA,
886 Sigurdsson A, Jonasdottir A, Jonasdottir A et al. 2012. Rate of de novo mutations and
887 the importance of father's age to disease risk. *Nature* **488**: 471-475.
888 Lamarre S, Frasse P, Zouine M, Labourdette D, Sainderichin E, Hu G, Le Berre-Anton V,
889 Bouzayen M, Maza E. 2018. Optimization of an RNA-Seq Differential Gene Expression
890 Analysis Depending on Biological Replicate Number and Library Size. *Front Plant Sci*
891 **9**: 108.
892 Langmead B, Trapnell C, Pop M, Salzberg SL. 2009. Ultrafast and memory-efficient alignment
893 of short DNA sequences to the human genome. *Genome Biol* **10**: R25.
894 LaRocca TJ, Cavalier AN, Wahl D. 2020. Repetitive elements as a transcriptomic marker of
895 aging: Evidence in multiple datasets and models. *Aging Cell* **19**: e13167.
896 Liao Y, Smyth GK, Shi W. 2014. featureCounts: an efficient general purpose program for
897 assigning sequence reads to genomic features. *Bioinformatics* **30**: 923-930.
898 Lin KY, Wang WD, Lin CH, Rastegari E, Su YH, Chang YT, Liao YF, Chang YC, Pi H, Yu BY et al.
899 2020. Piwi reduction in the aged niche eliminates germline stem cells via Toll-GSK3
900 signaling. *Nat Commun* **11**: 3147.
901 Liu Y, Kassack ME, McFaul ME, Christensen LN, Siebert S, Wyatt SR, Kamei CN, Horst S,
902 Arroyo N, Drummond IA et al. 2022. Single-cell transcriptome reveals insights into
903 the development and function of the zebrafish ovary. *Elife* **11**.
904 Love MI, Huber W, Anders S. 2014. Moderated estimation of fold change and dispersion for
905 RNA-seq data with DESeq2. *Genome Biol* **15**: 550.

906 Malki S, van der Heijden GW, O'Donnell KA, Martin SL, Bortvin A. 2014. A role for
907 retrotransposon LINE-1 in fetal oocyte attrition in mice. *Dev Cell* **29**: 521-533.
908 Mani SR, Juliano CE. 2013. Untangling the web: the diverse functions of the PIWI/piRNA
909 pathway. *Mol Reprod Dev* **80**: 632-664.
910 McClintock B. 1984. The significance of responses of the genome to challenge. *Science* **226**:
911 792-801.
912 Mira A. 1998. Why is meiosis arrested? *J Theor Biol* **194**: 275-287.
913 Naumann B, Englert C. 2018. Dispersion/reaggregation in early development of annual
914 killifishes: Phylogenetic distribution and evolutionary significance of a unique
915 feature. *Dev Biol* **442**: 69-79.
916 Pantano L. 2022. DEGreport: Report of DEG analysis. R package version 1.30.3., Vol 2022, p.
917 DEGreport: Report of DEG analysis. R package version 1.30.33.
918 Perheentupa A, Huhtaniemi I. 2009. Aging of the human ovary and testis. *Mol Cell*
919 *Endocrinol* **299**: 2-13.
920 Quinlan AR, Hall IM. 2010. BEDTools: a flexible suite of utilities for comparing genomic
921 features. *Bioinformatics* **26**: 841-842.
922 Reichwald K, Petzold A, Koch P, Downie BR, Hartmann N, Pietsch S, Baumgart M, Chalopin D,
923 Felder M, Bens M et al. 2015. Insights into Sex Chromosome Evolution and Aging
924 from the Genome of a Short-Lived Fish. *Cell* **163**: 1527-1538.
925 Roovers EF, Rosenkranz D, Mahdipour M, Han CT, He N, Chuva de Sousa Lopes SM, van der
926 Westerlaken LA, Zischler H, Butter F, Roelen BA et al. 2015. Piwi proteins and piRNAs
927 in mammalian oocytes and early embryos. *Cell Rep* **10**: 2069-2082.

928 Rosenberg AM, Rausser S, Ren J, Mosharov EV, Sturm G, Ogden RT, Patel P, Kumar Soni R,
929 Lacefield C, Tobin DJ et al. 2021. Quantitative mapping of human hair greying and
930 reversal in relation to life stress. *Elife* **10**.
931 Rosenkranz D, Zischler H. 2012. proTRAC--a software for probabilistic piRNA cluster
932 detection, visualization and analysis. *BMC Bioinformatics* **13**: 5.
933 Sahu S, Dattani A, Aboobaker AA. 2017. Secrets from immortal worms: What can we learn
934 about biological ageing from the planarian model system? *Semin Cell Dev Biol* **70**:
935 108-121.
936 Sargent KM, McFee RM, Spuri Gomes R, Cupp AS. 2015. Vascular endothelial growth factor
937 A: just one of multiple mechanisms for sex-specific vascular development within the
938 testis? *J Endocrinol* **227**: R31-50.
939 Schaible R, Scheuerlein A, Danko MJ, Gampe J, Martinez DE, Vaupel JW. 2015. Constant
940 mortality and fertility over age in Hydra. *Proc Natl Acad Sci U S A* **112**: 15701-15706.
941 Shao F, Wang J, Xu H, Peng Z. 2018. FishTEDB: a collective database of transposable
942 elements identified in the complete genomes of fish. *Database (Oxford)* **2018**.
943 Sharov AA, Falco G, Piao Y, Poosala S, Becker KG, Zonderman AB, Longo DL, Schlessinger D,
944 Ko M. 2008. Effects of aging and calorie restriction on the global gene expression
945 profiles of mouse testis and ovary. *BMC Biol* **6**: 24.
946 Simon M, Van Meter M, Ablaeva J, Ke Z, Gonzalez RS, Taguchi T, De Cecco M, Leonova KI,
947 Kogan V, Helfand SL et al. 2019. LINE1 Derepression in Aged Wild-Type and SIRT6-
948 Deficient Mice Drives Inflammation. *Cell Metab* **29**: 871-885 e875.
949 Smit A, Hubley, R & Green, P. . 2013-2015. RepeatMasker Open-4.0.
950 <http://www.repeatmasker.org>. Accessed August 20, 2021.

951 Sousa-Victor P, Ayyaz A, Hayashi R, Qi Y, Madden DT, Lunyak VV, Jasper H. 2017. Piwi Is
952 Required to Limit Exhaustion of Aging Somatic Stem Cells. *Cell Rep* **20**: 2527-2537.
953 Suzuki R, Shimodaira H. 2006. Pvclust: an R package for assessing the uncertainty in
954 hierarchical clustering. *Bioinformatics* **22**: 1540-1542.
955 Teefy BB, Siebert S, Cazet JF, Lin H, Juliano CE. 2020. PIWI-piRNA pathway-mediated
956 transposable element repression in Hydra somatic stem cells. *RNA* **26**: 550-563.
957 Terzibasi Tozzini E, Cellerino A. 2020. Nothobranchius annual killifishes. *Evodevo* **11**: 25.
958 Thomson T, Lin H. 2009. The biogenesis and function of PIWI proteins and piRNAs: progress
959 and prospect. *Annu Rev Cell Dev Biol* **25**: 355-376.
960 Valenzano DR, Benayoun BA, Singh PP, Zhang E, Etter PD, Hu CK, Clement-Ziza M, Willemsen
961 D, Cui R, Harel I et al. 2015. The African Turquoise Killifish Genome Provides Insights
962 into Evolution and Genetic Architecture of Lifespan. *Cell* **163**: 1539-1554.
963 Valenzano DR, Sharp S, Brunet A. 2011. Transposon-Mediated Transgenesis in the Short-
964 Lived African Killifish Nothobranchius furzeri, a Vertebrate Model for Aging. *G3*
965 *(Bethesda)* **1**: 531-538.
966 Vandewege MW, Patt RN, 2nd, Merriman DK, Ray DA, Hoffmann FG. 2022. The PIWI/piRNA
967 response is relaxed in a rodent that lacks mobilizing transposable elements. *RNA* **28**:
968 609-621.
969 Vrtilek M, Zak J, Blazek R, Polacik M, Cellerino A, Reichard M. 2018a. Limited scope for
970 reproductive senescence in wild populations of a short-lived fish.
971 *Naturwissenschaften* **105**: 68.
972 Vrtilek M, Zak J, Psenicka M, Reichard M. 2018b. Extremely rapid maturation of a wild
973 African annual fish. *Curr Biol* **28**: R822-R824.

974 Wang W, Han BW, Tipping C, Ge DT, Zhang Z, Weng Z, Zamore PD. 2015. Slicing and Binding
975 by Ago3 or Aub Trigger Piwi-Bound piRNA Production by Distinct Mechanisms. *Mol*
976 *Cell* **59**: 819-830.
977 Watanabe T, Totoki Y, Toyoda A, Kaneda M, Kuramochi-Miyagawa S, Obata Y, Chiba H,
978 Kohara Y, Kono T, Nakano T et al. 2008. Endogenous siRNAs from naturally formed
979 dsRNAs regulate transcripts in mouse oocytes. *Nature* **453**: 539-543.
980 Willemsen D, Cui R, Reichard M, Valenzano DR. 2020. Intra-species differences in population
981 size shape life history and genome evolution. *Elife* **9**.
982 Yamashiro H, Siomi MC. 2018. PIWI-Interacting RNA in Drosophila: Biogenesis, Transposon
983 Regulation, and Beyond. *Chem Rev* **118**: 4404-4421.
984 Yang N, Srivastav SP, Rahman R, Ma Q, Dayama G, Li S, Chinen M, Lei EP, Rosbash M, Lau
985 NC. 2022. Transposable element landscapes in aging Drosophila. *PLoS Genet* **18**:
986 e1010024.
987 Zak J, Reichard M. 2021. Reproductive senescence in a short-lived fish. *J Anim Ecol* **90**: 492-
988 502.
989 Zhang P, Kang JY, Gou LT, Wang J, Xue Y, Skogerboe G, Dai P, Huang DW, Chen R, Fu XD et al.
990 2015. MIWI and piRNA-mediated cleavage of messenger RNAs in mouse testes. *Cell*
991 *Res* **25**: 193-207.
992
993
994

995 **Legends to Figures**

996 **Figure 1. A study of gonadal aging in the naturally short-lived African turquoise**
997 **killifish**

998 **(A)** Experimental scheme for killifish gonad sequencing. Killifish gonads (N = 5) were
999 dissected and total RNA was extracted. Only high quality RNA samples (RIN>7) were
1000 included for further processing (see **Supplemental Fig. S1A**). Small RNA and mRNA RNA-
1001 seq libraries were derived from each total RNA sample and sequenced for downstream
1002 analyses. **(B)** Lifespan curve for female and male GRZ strain killifish at the USC Benayoun
1003 lab facility. GRZ females lived significantly longer than males (p = 0.002; log Rank test).
1004 Median lifespan of females: 26.55 weeks, males: 19.4 weeks. Vertical dotted lines: ages
1005 sampled in this study (5, 10, 15 weeks), chosen to represent aging before substantially
1006 decreased population survival. **(C-E)** Principal component analyses [PCAs] for **(C)** mRNA
1007 gene expression **(D)** TE expression and **(E)** TE-mapping piRNA abundance (see methods).
1008

1009 **Figure 2. Differential gene expression analysis and GO Biological Process functional**
1010 **enrichment analysis with ovarian aging.**

1011 **(A)** Scheme used for differential gene expression [DGE] analysis used in this study. DGE
1012 was performed with DESeq2's likelihood ratio testing [LRT], which revealed 4 approximate
1013 groups of differentially expressed genes corresponding to expression (a) Down at Middle-
1014 Age, (b) Up at Middle-Age, (c) Down with Age and (d) Up with Age. **(B)** Heatmaps of gene
1015 expression for genes significantly regulated with age in aging killifish ovaries by DEseq2 LRT
1016 (FDR < 1e-6). Most differentially expressed genes transiently changed at middle-age. **(C)**
1017 Functional enrichment analysis for each gene cluster in **Fig. 2B**, showing the top 10 most
1018 significant GO "Biological Process" terms by 'GOstats' (FDR < 5%; see **Supplemental**
1019 **Table S3A** for complete list of enriched terms). The most significant term downregulated in
1020 middle-aged ovaries is "piRNA metabolic process" (bolded). FDR: False discovery rate.
1021 Enrichment: fold enrichment over background.
1022

Figure 3. Differential gene expression and GO Biological Process functional enrichment analysis with testicular aging.

(A) Heatmaps of gene expression for genes significantly regulated with age in aging killifish testes by DEseq2 LRT (FDR < 1e-6). Groups correspond to those defined in **Fig. 2A**. Like ovaries, most differential gene expression in killifish testes occurs transiently at middle-age. **(B)** Functional enrichment analysis for each gene cluster shown in **Fig. 3A** showing the top 10 most significant GO "Biological Process" terms by 'GOstats' (FDR < 5%; see **Supplemental Table S3D** for complete list of enriched terms). Genes that are upregulated in middle-age testis are enriched for terms related to spermatogenesis. Note that cluster (d) (genes up with age) had too few genes to generate meaningful enrichment results. FDR: False discovery rate. Enrichment: fold enrichment over background.

Figure 4. TE expression dynamics in the aging turquoise killifish gonad.

(A) Experimental scheme for TE transcriptional analysis in aging gonads. Fractional TE counts were computed by counting the number of TE counts over total assigned mRNA-seq counts (genes and TEs). TE DGE was conducted in the same manner as the genic DGE analysis (see methods), and were labelled with the cluster nomenclature from **Fig. 2A**. **(B)** Proportion of assigned reads allocated to TEs from each mRNA-seq library for ovaries and testes. Significance in non-parametric Wilcoxon Rank Sum test. Note that old ovaries have significantly fewer proportional TE counts relative to middle-aged ovaries, and that testes seem to show a marginal increase in TE transcription with aging. **(C)** Heatmaps of mRNA expression for TEs significantly regulated with age in aging killifish ovaries by DEseq2 LRT (FDR < 1e-6). Each TE family is color-coded by row, revealing no obvious bias or enrichment for a specific TE type. **(D)** Heatmaps of mRNA expression for TEs significantly regulated with age in aging killifish testes by DEseq2 LRT (FDR < 1e-6). The only age differentially regulated TEs in the turquoise killifish testis are transiently upregulated at middle-age.

Figure 5. PIWI pathway activity and piRNA abundance characterization in aging turquoise killifish gonads.

(A) Heatmaps of normalized gene expression from ovaries and testes with aging in the GO "piRNA metabolic pathway" term. Killifish gene names and their best human homologs are indicated for each row. Rows were normalized by the median expression level in the cognate young gonad, so as to facilitate visualization of age-related changes. Genes involved in this pathway tend to be significantly downregulated in middle-aged ovaries (see **Fig. 2C**). **(B)** Sequence logo plots of piRNA nucleotide composition from ovaries and testes, using data for each gonad type pooled across ages and replicates. As expected for piRNAs, killifish piRNAs show a strong position 1-U bias. There is also a slight bias for Adenine at position 10, consistent with active ping-pong biogenesis in killifish gonads. **(C)** Stacked barplots depicting the TE family composition of piRNA clusters and the killifish genome, as a percentage of identified elements. The piRNA cluster TE composition is broadly reflective of the TE composition of the genome. **(D)** Heatmaps of TE-targeted piRNA abundance for TEs significantly regulated with age in aging killifish ovaries by DEseq2 LRT (FDR < 1e-6). TE family is color-coded for each row. In ovaries, most differentially piRNA-targeted TEs show a decrease of piRNA counts at middle-age. **(E)** Heatmaps of TE-targeted piRNA abundance for TEs significantly regulated with age in aging killifish testes by DEseq2 LRT (FDR < 1e-6). **(F)** Venn diagram of the overlap between TE_mapping piRNAs significantly upregulated in middle-age ovaries (see **Fig. 5D**; pattern a) and TEs that are significantly downregulated in middle-age ovaries (see **Fig. 4C**; pattern b). Significance for the overlap being larger than expected by chance was calculated using Fisher's exact test, compared to TEs detected in both analyses. A pie chart of the composition of "consistent" TEs is also reported.

Figure 6. Analysis of ping-pong biogenesis in aging turquoise killifish gonads.

(A) Explanatory diagram of ping-pong biogenesis. PIWI1 (the PIWI protein loaded with 'primary' piRNAs complementary to TEs) binds to and cleaves a TE mRNA species. The cleaved TE mRNA is loaded into PIWI2 (the PIWI protein loaded with cleaved TE fragments,

or 'TE-derived secondary' piRNAs). PIWI proteins always cleave their targets 10 basepairs from the 5' end of the piRNA. This mechanism, known as ping-pong biogenesis, will generate a preponderance of complementary piRNAs with a 10 basepair overlap, the detection of which is the basis of the assays shown in **Fig. 6B-F**. **(B)** Boxplot showing the median frequency of 10 basepair overlaps for 1 million piRNA reads over 100 bootstraps per biological sample (ppr-mbr: Ping-Pong Reads per Million Bootstrapped Reads,) as generated by PPmeter. Age groups within each sex were compared using the non-parametric Wilcoxon rank sum test. **(C)** Boxplot showing median Z_{10} scores over consensus TEs for each biological sample. Z_{10} scores are an alternative measure of ping-pong. Non-parametric Wilcoxon Rank Sum tests were used to test for significant differences between age groups. **(D)** Schematic for analysis of differential Z_{10} score patterns with gonadal aging. Z_{10} scores were generated for each consensus TE sequence in FishTEDB in each biological sample. An ANOVA test was run to detect any significant differences in Z_{10} score between age groups within each sex (FDR < 5%). Significant TEs were assigned to groups based on expression dynamics that align to the broad groups defined in **Fig. 2A**, with the detection of 2 new subgroups showing minimal expression at middle-age (a_1 and a_2), with highest Z_{10} scores in the young samples and old samples, respectively. **(E)** Heatmaps of differential Z_{10} scores with age in aging killifish ovaries by ANOVA (FDR < 5%). **(F)** Heatmaps of differential Z_{10} scores with age in aging killifish testes by ANOVA (FDR < 5%). A roughly equivalent amount of consensus TE sequences show linear up- and downregulation with age. The cognate TE family is color-coded by row, and does not reveal any specific bias.

Figure 1

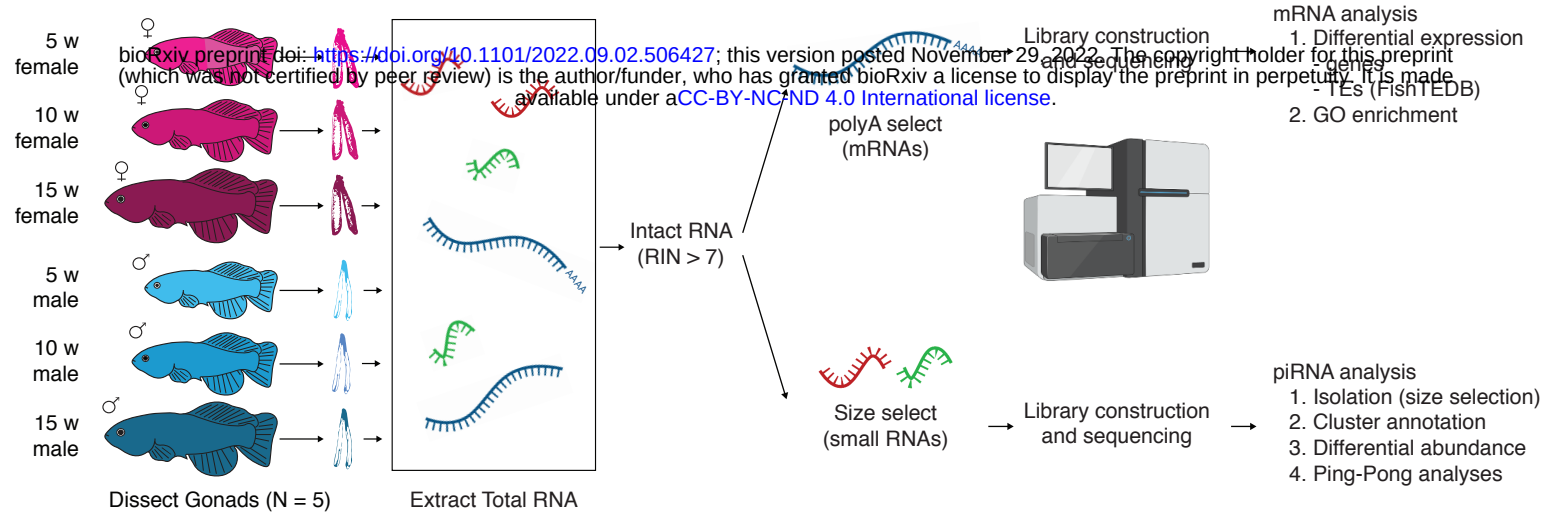

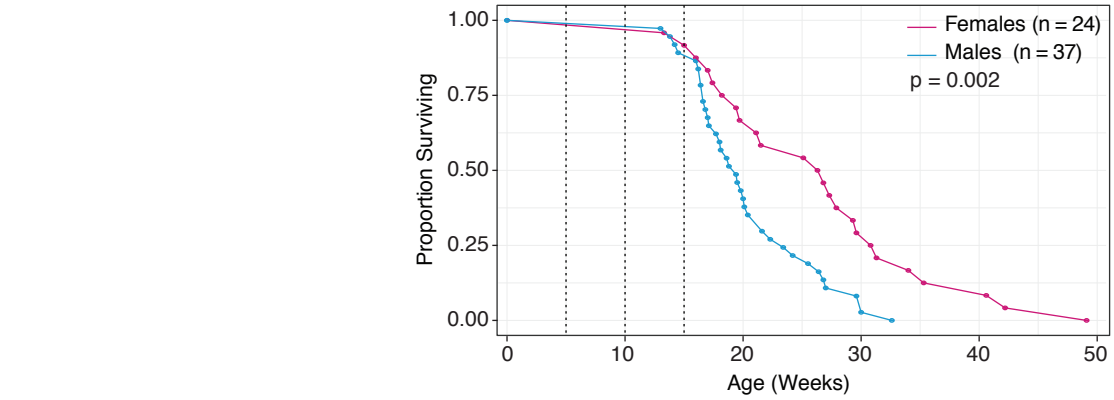

Figure 2

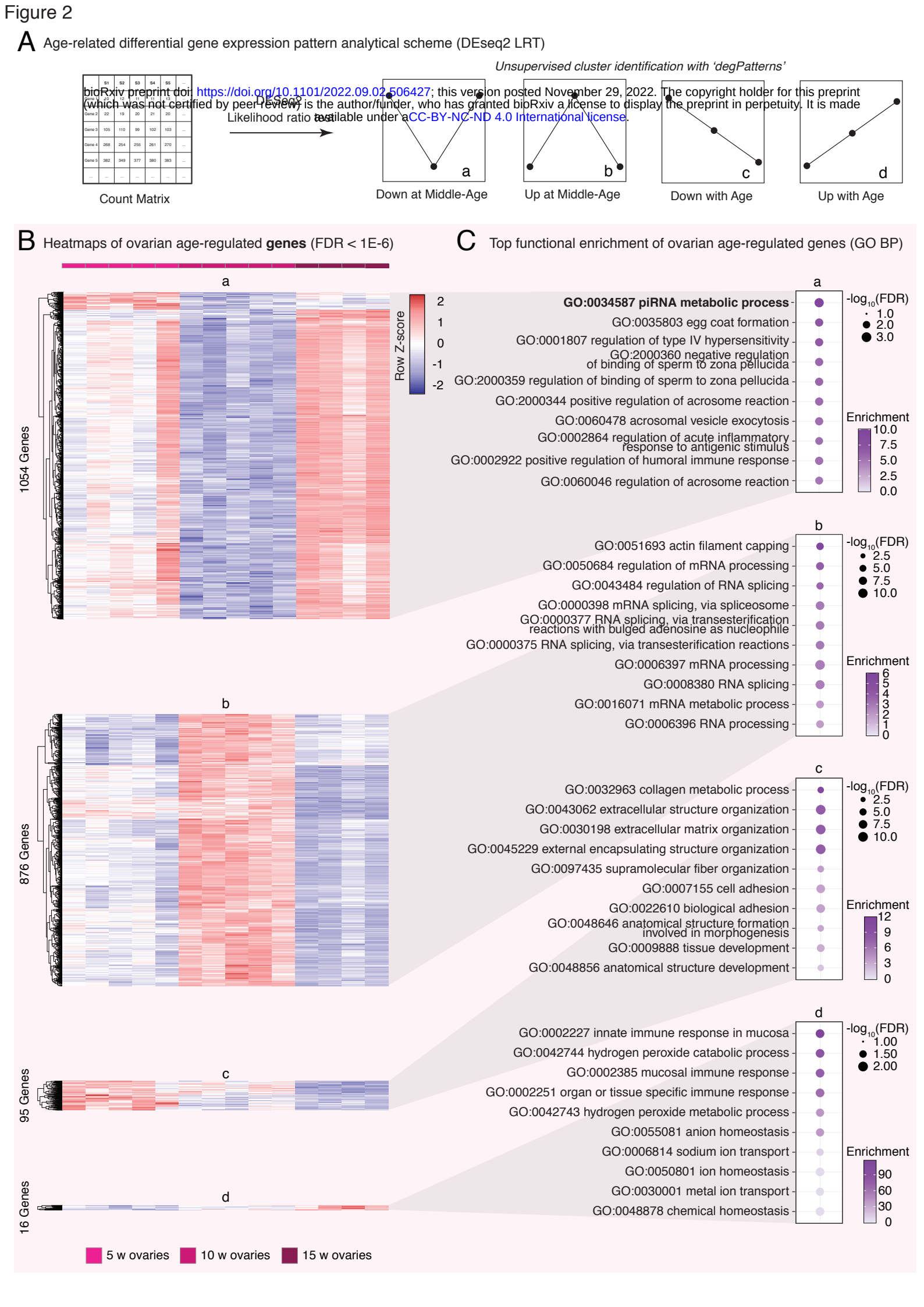

Figure 3

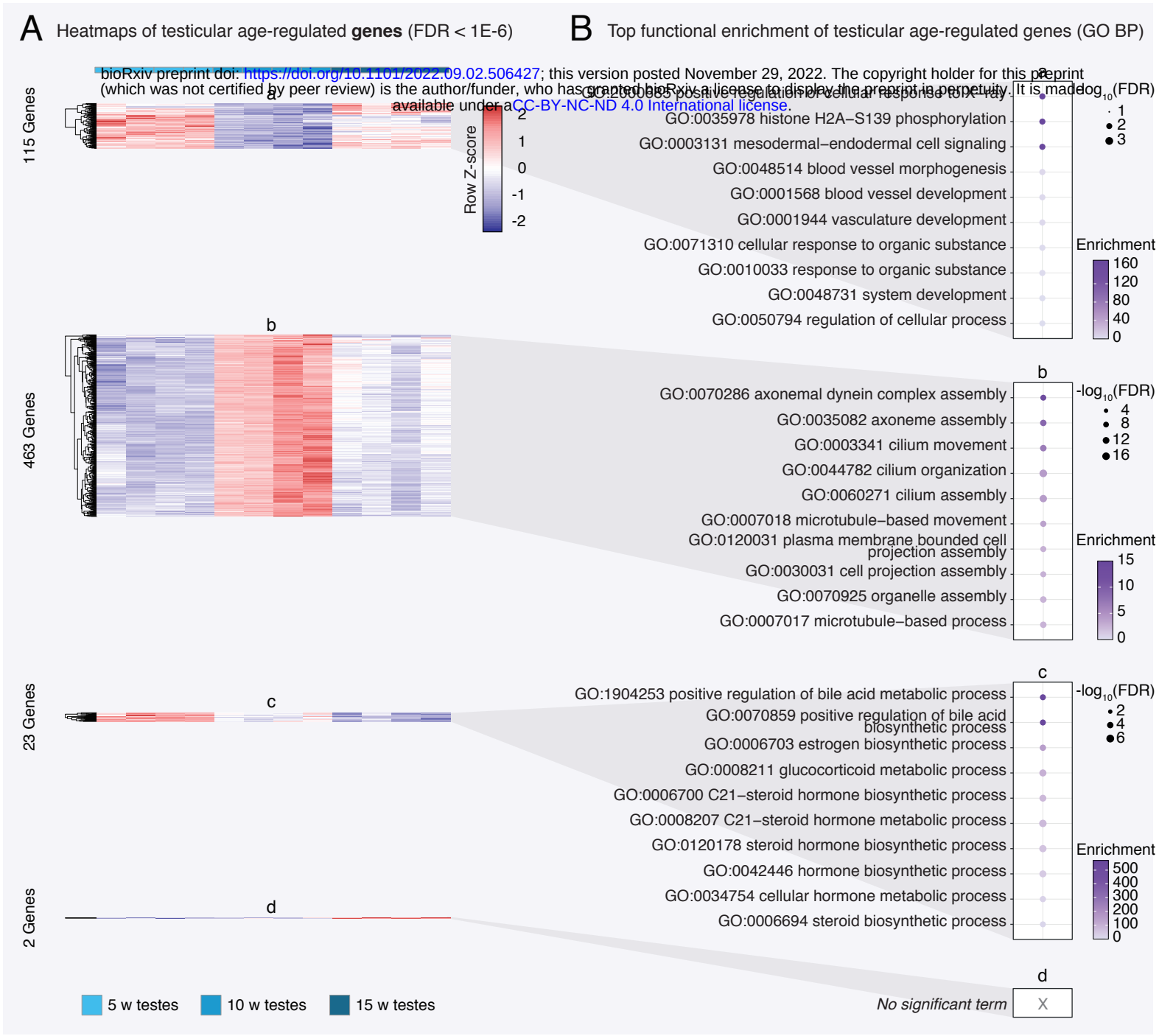

Figure 4

A Scheme of gonadal TE expression analysis

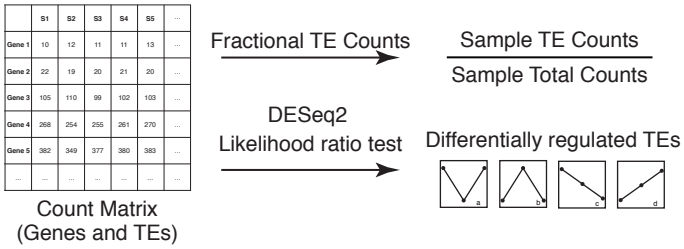

B Fraction of mapped reads aligned to TE sequence in gonadal mRNA

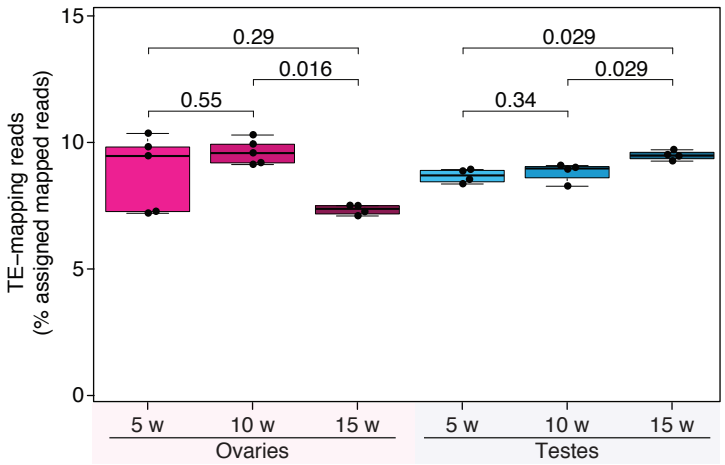

C Heatmaps of ovary age-regulated **TEs** (FDR < 1E-6)

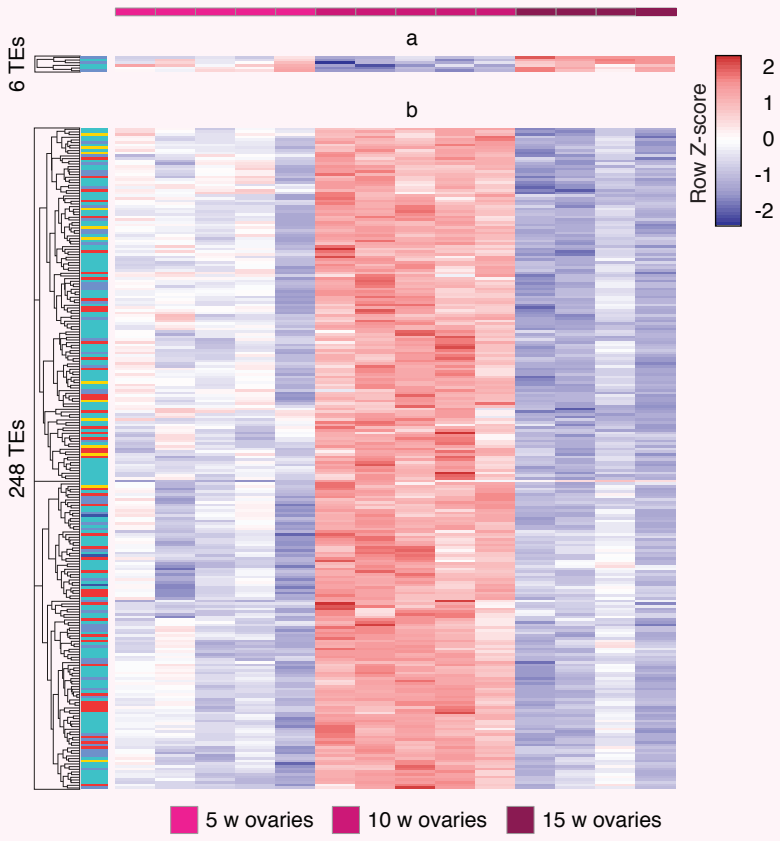

D Heatmap of testes age-regulated **TEs** (FDR < 1E-6)

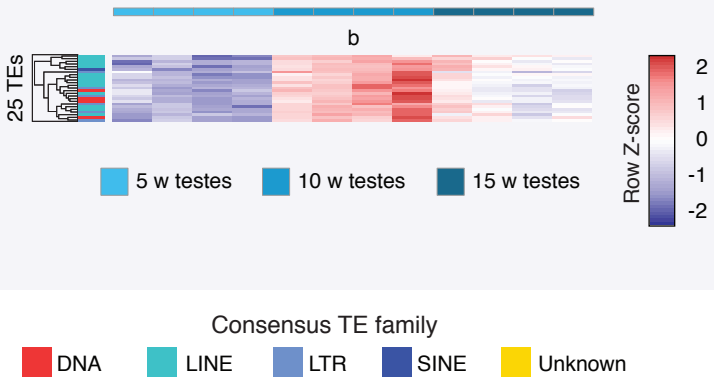

Figure 5

A Heatmap of gonadal expression for genes in "piRNA metabolic pathway" (GO:0034587)

B Gonadal piRNA nucleotide composition (pooled ages)

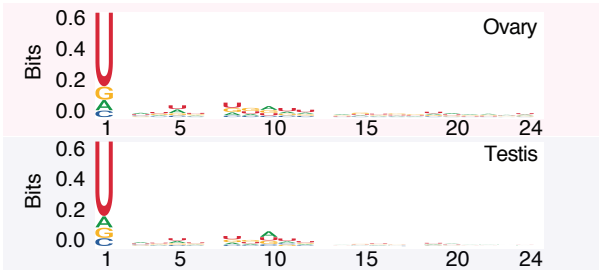

C TE sequence composition of genome and piRNA clusters

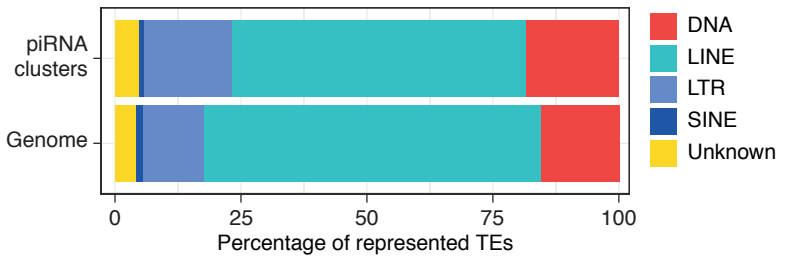

D Heatmaps of ovary age-regulated **TE-mapping piRNAs** (FDR < 1E-6)

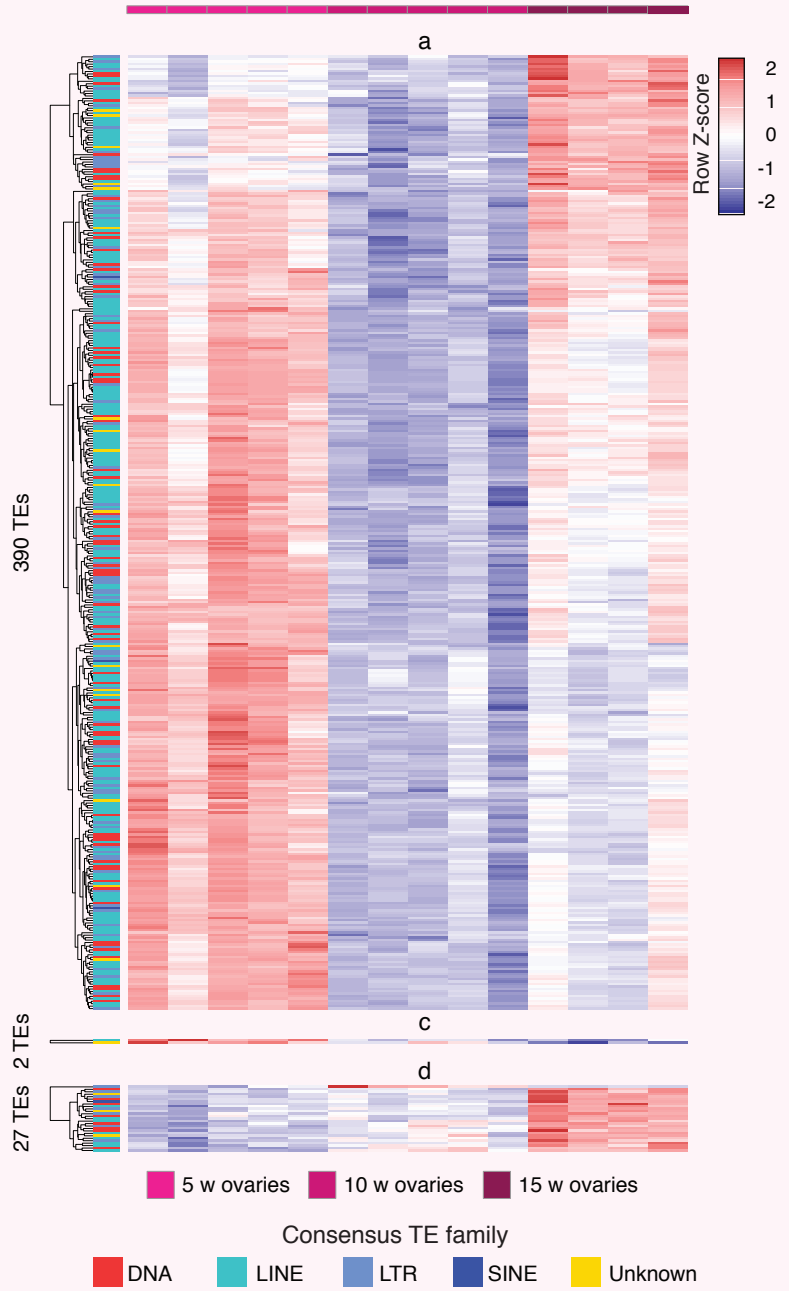

E Heatmaps of testes age-regulated **TE-mapping piRNAs** (FDR < 1E-6)

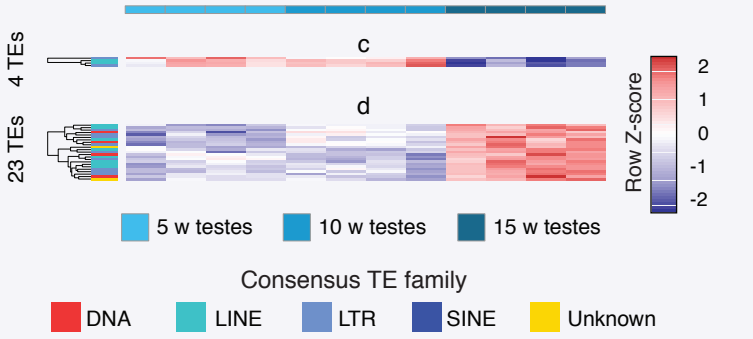

F Ovarian age-regulated of **TEs** *vs.* **TE-mapping piRNAs** (FDR < 1E-6)

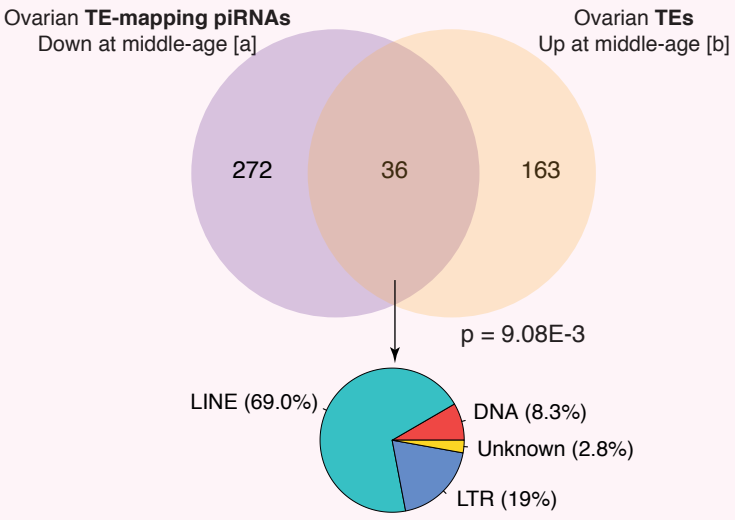

Figure 6

A Ping–pong mechanism

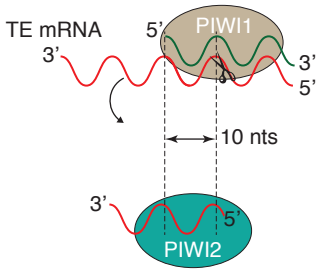

B Longitudinal ping-pong rate over consensus TEs

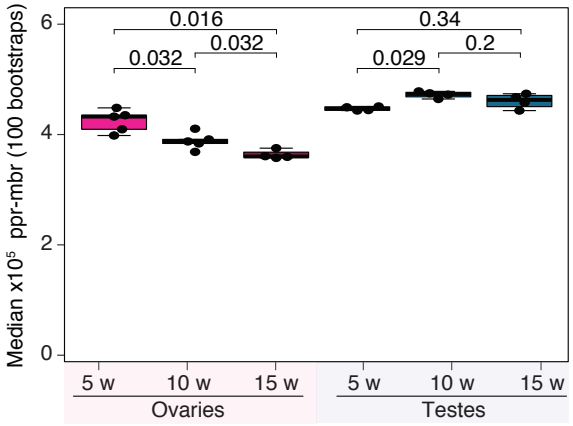

C Median Z_{10} score over consensus TEs

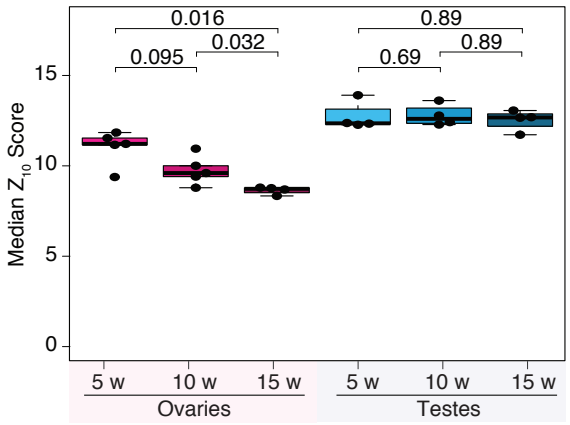

D Age-related differential Z_{10} ping-pong pattern analysis (ANOVA)

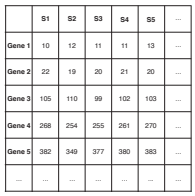

Z_{10} Score Matrix

ANOVA (FDR < 5%)

Unsupervised cluster identification with 'degPatterns'

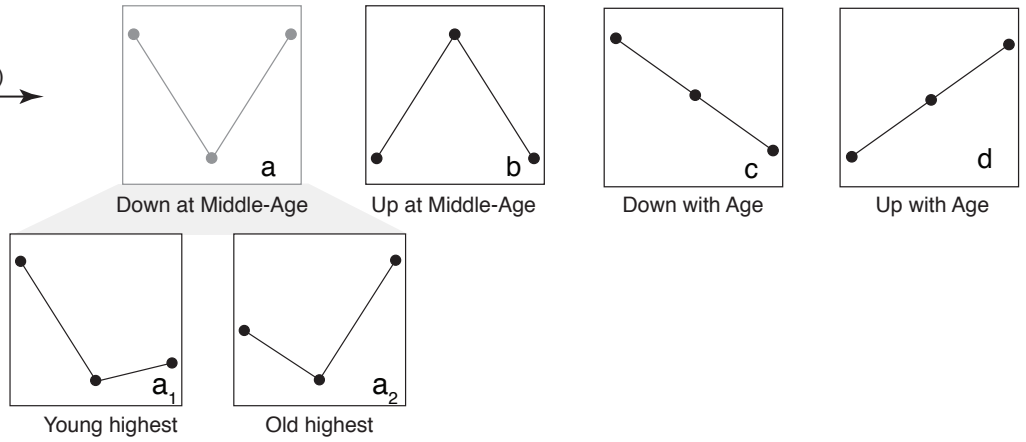

E Heatmaps of ovary **ping-pong targeted TE Z_{10} scores** (FDR < 5%)

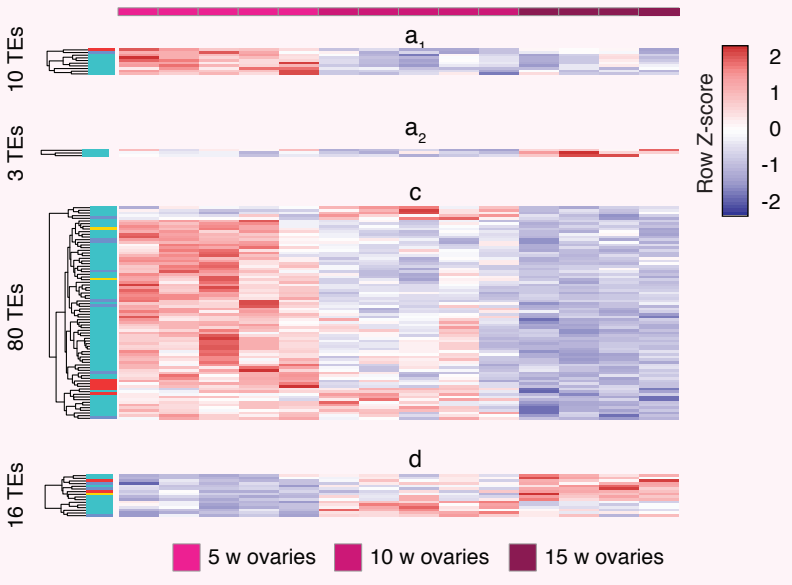

F Heatmaps of testes **ping-pong targeted TE Z_{10} scores** (FDR < 5%)